CANCER IMMUNOLOGY

Proximity-dependent labeling identifies dendritic cells that drive the tumor-specific CD4+ T cell response

Aleksey Chudnovskiy[1]*†, Tiago B. R. Castro[1], Sandra Nakandakari-Higa[1], Ang Cui[2,3,4], Chia-Hao Lin[5,6], Moshe Sade-Feldman[2], Brooke K. Phillips[1], Juhee Pae[1], Luka Mesin[1], Juliana Bortolatto[1], Lawrence D. Schweitzer[2], Giulia Pasqual[7,8], Li-Fan Lu[5,6], Nir Hacohen[2,9], Gabriel D. Victora[1]*

Dendritic cells (DCs) are uniquely capable of transporting tumor antigens to tumor-draining lymph nodes (tdLNs) and interact with effector T cells in the tumor microenvironment (TME) itself, mediating both natural antitumor immunity and the response to checkpoint blockade immunotherapy. Using LIPSTIC (Labeling Immune Partnerships by SorTagging Intercellular Contacts)–based single-cell transcriptomics, we identified individual DCs capable of presenting antigen to CD4+ T cells in both the tdLN and TME. Our findings revealed that DCs with similar hyperactivated transcriptional phenotypes interact with helper T cells both in tumors and in the tdLN and that checkpoint blockade drugs enhance these interactions. These findings show that a relatively small fraction of DCs is responsible for most of the antigen presentation in the tdLN and TME to both CD4+ and CD8+ tumor–specific T cells and that classical checkpoint blockade enhances CD40-driven DC activation at both sites.

INTRODUCTION

When properly activated, T cells can exert powerful control over cancer, as evidenced by decades of work that culminated in checkpoint blockade immunotherapies (1–3). As with other adaptive immune processes, the quality of the T cell response toward a tumor is heavily dependent on the identity and phenotype of the dendritic cells (DCs) that present tumor-derived antigen to T cells in the tumor-draining lymph node (tdLN). tdLN DCs are divided into migratory DCs, capable of transporting antigens acquired in the tumor to the tdLN, and resident DCs, which have access only to antigen that arrives to the LN through lymphatics or that is carried by their migratory counterparts (4–7). Both populations can be further subdivided along an orthogonal axis into conventional cDC1 and cDC2 subsets on the basis of their phenotype and ontogeny (5, 8). In general, cDC1s have higher capacity to prime CD8+ T cells, whereas migratory cDC2s are best at priming CD4+ T cells (9–11), although these distinctions are not absolute (12).

Both cDC1s and cDC2s have been implicated as drivers of the antitumor immune response (9, 13). Mice lacking cDC1s show enhanced tumor growth concomitant with reduced tumor-specific effector CD8+ T cells (11, 14–17). CD4+ T cell priming by cDC2s is suppressed by regulatory T (Treg) cells (18), and Treg depletion unleashes a cDC2-driven CD4+ T cell response to the tumor (13). Moreover, immune checkpoint inhibitors do not work efficiently in the absence of DCs, highlighting the role of antigen presentation as a major driver of the response to immunotherapy (11, 15, 19). More recent studies have identified a previously undescribed DC state termed mature DCs enriched in immunoregulatory molecules (mRegDCs) (20). DCs in this state have enhanced capacity to take up antigens but reduced ability to prime antitumor T cell responses. mRegDCs share many common genes with the cDC3 subset described in humans (21, 22), and further work is needed to delineate the cDC3 and mRegDC states (23).

DCs are also present in the tumor microenvironment (TME), where they can interact with both effector and Treg cells, further shaping antitumor immunity. However, given the heterogeneity of DC phenotypes in the TME, as well as the presence of other populations of non-DC antigen-presenting cells (APCs) in the tumor, determining which DC populations contribute to antitumor T cell responses remains a challenge (24–26). Assessing the contribution of specific APC subsets to T cell activity in the tumor is particularly challenging because most if not all T cells arriving in the TME have already been primed in the tdLN; therefore, the relative contribution of local TME and distal tdLN APCs to T cell activity is difficult to discriminate (24–27). To address these types of questions, we previously developed LIPSTIC (Labeling Immune Partnerships by SorTagging Intercellular Contacts), a proximity-based labeling method based on transfer between interacting cells of a labeled substrate detectable by flow cytometry that allows identification and isolation of DCs engaged in antigen presentation to T cells in vivo (28). By combining LIPSTIC with single-cell RNA sequencing (scRNA-seq), we performed interaction-based transcriptomic profiling of the DCs responsible for presenting tumor-derived antigen to cognate CD4+ T cells in the tdLN and of the myeloid cells that engage with any CD4+ T cells in the TME. Our data show that a minor population of DCs, characterized by a hyperactivated transcriptional program, accounted for most antigen presentation to CD4+ T cells in the tdLN, a phenotype that was shared with the DCs that interacted with effector CD4+ T cells in the TME. T cell–DC interactions in both sites were increased by checkpoint blockade with anti–cytotoxic T lymphocyte associated protein 4 (CTLA-4) antibodies. Together, our data indicate that DCs with similar hyperactivated

[1]Laboratory of Lymphocyte Dynamics, Rockefeller University, New York, NY, USA. [2]Broad Institute of MIT and Harvard, Cambridge, MA, USA. [3]Harvard School of Dental Medicine, Harvard University, Boston, MA, USA. [4]Harvard Medical School, Boston, MA, USA. [5]School of Biological Sciences, University of California, San Diego, La Jolla, CA, USA. [6]Moores Cancer Center, University of California, San Diego, La Jolla, CA, USA. [7]Laboratory of Synthetic Immunology, Oncology and Immunology Section, Department of Surgery Oncology and Gastroenterology, University of Padua, Padua, Italy. [8]Veneto Institute of Oncology IOV-IRCCS, Padua, Italy. [9]Center for Cancer Research, Massachusetts General Hospital, Boston, MA, USA.
*Corresponding author. Email: aleksey.chudnovskiy@crick.ac.uk (A.C.); victora@rockefeller.edu (G.D.V.)
†Present address: Francis Crick Institute, London, UK.

transcriptional phenotypes interact with helper T cells in both tumors and the tdLN and that checkpoint blockade drugs enhance these interactions.

RESULTS

LIPSTIC identifies DCs that present tumor antigen to naïve CD4+ T cells in vivo

LIPSTIC relies on the *Staphylococcus aureus* transpeptidase sortase A (SrtA) to transfer an injectable biotinylated peptide substrate (biotin-LPETG) between pairs of cells interacting by the CD40L-CD40 pathway. SrtA, fused to the extracellular domain of CD40L expressed on CD4+ T cells, captures substrate injected in vivo and transfers it onto five N-terminal glycines engineered into the extracellular domain of CD40 (G_5-CD40) on interacting DCs (Fig. 1A). To apply this system to a solid tumor model, we engineered the B16 melanoma cell line to express the $OVA_{323-339}$ (OT-II) peptide (B16^{OT-II}; fig. S1A). We then inoculated G_5-CD40–expressing mice ($Cd40^{G5/G5}$) subcutaneously with 10^6 B16^{OT-II} cells in the flank region to generate a response in the tumor-draining inguinal lymph node. At 9 days postinjection (d.p.i.), we adoptively transferred 3×10^5 SrtA-expressing OT-II T cells (either carrying the conditional $Cd40lg^{SrtAv1}$ allele crossed to $Cd4$-Cre or carrying a constitutive $Cd40lg^{SrtAv2}$ allele; see Materials and Methods) into tumor-bearing mice. We performed LIPSTIC labeling of the tdLN by local injection of biotinylated LPETG substrate at 10 to 12 hours after T cell transfer (Fig. 1B), a point at which T cell interaction with DCs is exclusively cognate (*28*). This system allows transferred OT-II T cells to serve as "reporters" that specifically identify and label the subset of DCs capable of presenting antigen to naïve CD4+ T cells at that time point.

This approach revealed that a minor population (approximately 5 to 10%) of DCs acquired the LIPSTIC label in the tdLNs of mice bearing B16^{OT-II} tumors but not in controls inoculated with the parental B16 line [B16 wild type (WT)] (Fig. 1C). In agreement with previous findings (*10*, *28*), LIPSTIC labeling in the tdLN was detected exclusively on migratory (CD11c^{Int}MHC-II^{Hi}) but not resident (CD11c^{hi}MHC-II^{int}) DCs (Fig. 1D and fig. S1B). The specificity of LIPSTIC labeling was confirmed by injection of a blocking antibody to CD40L 2 hours before substrate injection, which fully abrogated labeling (Fig. 1E). Mixed bone marrow chimera experiments in which a fraction of DCs were deficient for major histocompatibility complex class II (MHC-II) confirmed that LIPSTIC captures predominantly interactions driven by antigen presentation in this setting (fig. S1C). Thus, LIPSTIC labeling in the B16 system is antigen specific and dependent on the CD40L-CD40 interaction. DCs of both XCR1+CD11b− (cDC1) and XCR1−CD11b+ (cDC2) phenotypes (Fig. 1F) were labeled by OT-II T cells, at a ratio that corresponded roughly to the total cDC2/cDC1 ratio in each tdLN. Thus, both subsets of DCs were equally capable of presenting tumor-derived antigens to specific CD4+ T cells in vivo, a finding supported by previous literature (*12*, *13*). Because our B16^{OT-II} cell line also expresses green fluorescent protein (GFP; fig. S1A), we were able to simultaneously probe DCs for interaction with CD4+ T cells and for the extent to which they carry intact tumor-derived proteins. Although there was a statistically significant enrichment in biotin+ cells among the GFP+ DC population, GFP and LIPSTIC labeling were overall poorly correlated (Fig. 1G). Thus, the storage of intact tumor-derived antigen does not overlap substantially with the ability to present this antigen to naïve CD4+ T cells in vivo, possibly

because of the specific kinetics of antigen storage and presentation over time.

To ascertain that biotin+ DCs carried the antigen necessary to drive proliferation of antigen-specific T cells, we set up a miniaturized assay in which 150 tdLN-derived biotin+ DCs were cocultured ex vivo with 750 carboxyfluorescein diacetate succinimidyl ester (CFSE)–labeled OT-II CD4+ T cells in the absence of exogenous antigen. This approach showed that biotin+ DCs were exclusively capable of driving T cell proliferation above the background levels obtained with DCs derived from mice carrying parental B16 melanomas that lacked the OT-II peptide (Fig. 1H). An analogous experiment with ovalbumin (OVA)–specific CD8+ (OT-I) T cells (using a B16 line that we engineered to express a transmembrane version of the full OVA protein, B16^{mOVA}) showed that, again, biotin+ tdLN DCs were exclusively capable of driving T cell proliferation (Fig. 1H). We conclude that LIPSTIC labeling faithfully identifies DCs in the tdLN that are capable of presenting antigen to both CD4+ and CD8+ T cells in vivo and that such DCs represent only a minor fraction of all DCs available at that site.

DCs that present tumor-derived antigens exhibit a distinct hyperactivated state

To understand what distinguishes DCs capable of presenting antigen to CD4+ T cells in tdLNs beyond a population-level analysis, we transcriptionally profiled individual biotin+ and biotin− migratory DCs obtained from tdLNs at 10 and 15 d.p.i. and control DCs from steady-state inguinal LNs (iLNs) using plate-based scRNA-seq. DCs fell into five transcriptional clusters (Fig. 2A and data file S1), of which two expressed signatures associated with a cDC1 phenotype (clusters 1 and 3) and three expressed a cDC2 phenotype (clusters 0, 2, and 4) (fig. S2A). Few differences were noted when comparing biotin− migratory DCs sorted from B16^{OT-II} tdLNs or total migratory DCs from steady-state iLNs. Conversely, biotin+ tdLN DCs, especially those with a cDC2 phenotype, were strongly enriched in cluster 0, which consisted almost exclusively of LIPSTIC-labeled cells (Fig. 2, B and C). Similar but less pronounced segregation of biotin+ and biotin− phenotypes was observed in cDC1 cluster 3 (Fig. 2B). In both cDC1 and cDC2 populations, LIPSTIC labeling correlated with expression of CD40 target genes (*29*), as expected given the pathway assayed by the LIPSTIC method (fig. S2B).

Differential gene expression comparing biotin+ and biotin− tdLN DCs showed statistically significant modulation of 269 genes (224 up-regulated and 45 down-regulated). Of these, 136 were commonly modulated in biotin+ cDC1 and cDC2 populations, and 66 changed exclusively in the biotin+ cDC2 population (fig. S2C and data file S2). Changes included up-regulation of genes encoding for classic markers of DC maturation (*Cd80*, *Cd86*, *Cd40*, and *Cd82*) and of nuclear factor κB activation [*Nfkbiz* and *Tnfaip3* (A20)] (*30*, *31*), typical of an activated DC state, as well as strong up-regulation of the inhibitory molecules *Cd200* and *Cd274* [encoding programmed cell death ligand 1 (PD-L1)] (Fig. 2D) (*20*, *32*). Genes functionally important for T cell priming were also up-regulated, including *Cd1d1*, the cytokines *Tnf* and *Ebi3*, drivers of DC–T cell interactions such as *Sema4a* and *Alcam* (*33*–*35*), and the proteasome activator involved in antigen presentation (*Psme2b*) (*36*), as were *Ifitm3*, *Tmem39a*, and *Tmem173* [stimulator of interferon genes (STING)], genes important for infectious disease and autoimmunity (*37*–*39*). LIPSTIC-labeled DCs, especially cDC2s, up-regulated several genes related to cell migration and microanatomical localization of DCs and T cells, including the
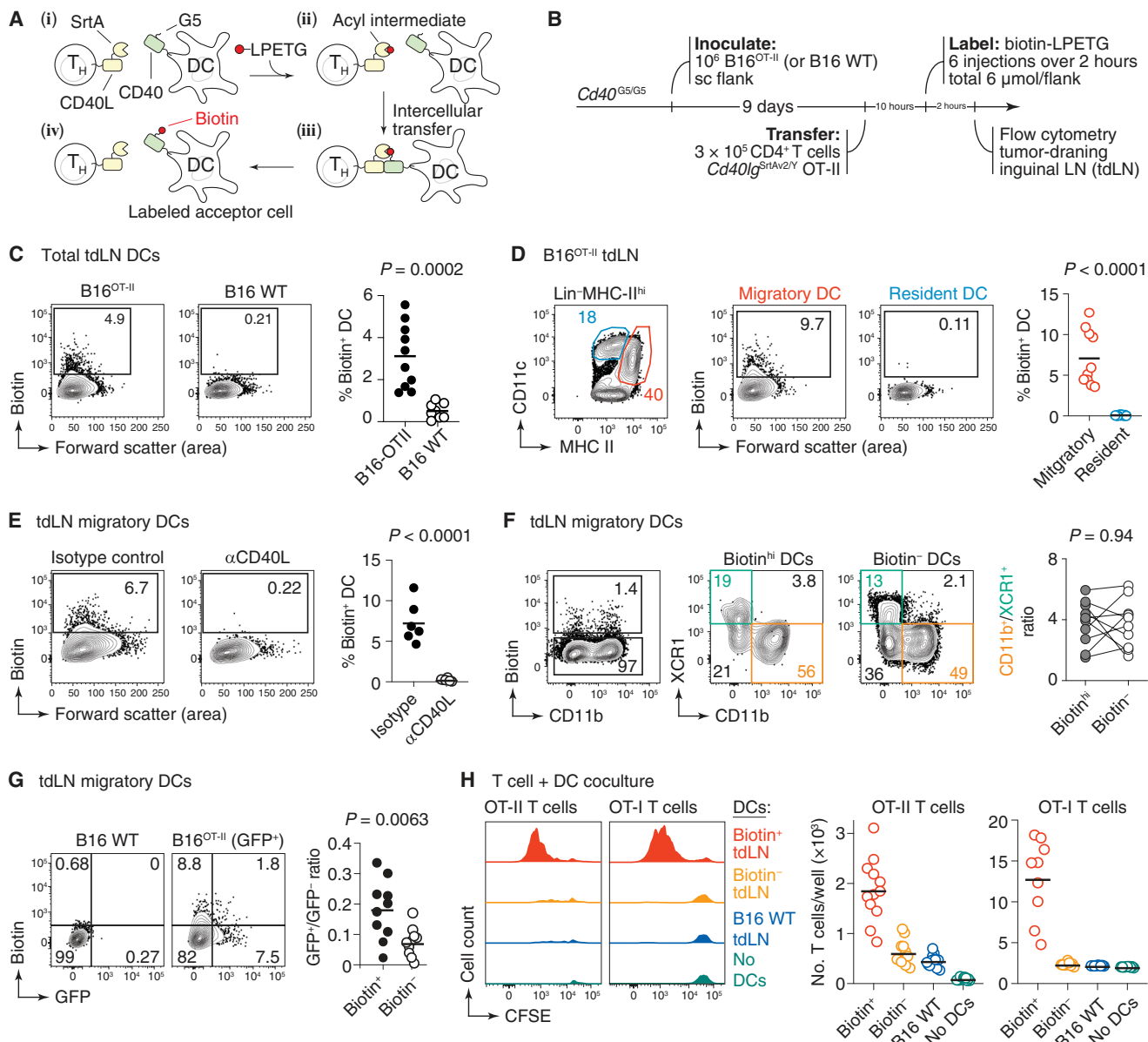
Fig. 1. Using LIPSTIC to identify tumor antigen–presenting DCs. (**A**) LIPSTIC schematic. T cells expressing SrtA fused to CD40L transfer an injectable biotin-LPETG onto five N-terminal glycines engineered into the extracellular domain of CD40 (G_5-CD40) on interacting DCs. (**B**) Setup for (C) to (G), except that in (F), donors carrying the $Cd40lg^{SrtAv1}$ conditional allele and $Cd4$-Cre were used. In (C), (D), and (G), bilateral tumors were injected, and each symbol represents one draining LN; in (E) and (F), each symbol represents one mouse. (**C**) Percentage of labeled DCs in mice bearing B16^{OTII} or parental B16 tumors (left) and quantification of data (right) (n = 5 or 4 mice per group from one experiment). (**D**) Percentage of labeled migratory and resident DCs in a tdLN, quantified on the right (n = 5 mice from one experiment). (**E**) Percentage of labeled DCs in mice treated with isotype control antibody versus anti-CD40L antibody (left), quantified on the right (n = 6 mice per group from one experiment). (**F**) Percentage of cDC1s and cDC2s among biotin$^+$ and biotin$^-$ DCs, quantified on the right (n = 10 mice from four experiments). (**G**) Percentage of GFP$^+$ and biotin$^+$ DCs in a tdLN (left) and quantification of GFP$^+$ DCs among biotin$^+$ and biotin$^-$ DCs in a tdLN (right; n = 5 mice from one experiment). (**H**) Proliferation of OT-II and OT-I T cells in vitro after 96 hours of coculture with DCs from mice carrying B16^{OTII} or B16^{OVA} tumors (left) and quantification of T cells per well at the end of the culture period (right). For (H), tdLNs were pooled from n = 6 to 10 mice; for OT-II, data were pooled from two experiments; for OT-I, data are from one experiment; each dot represents one culture well. P values are for unpaired t test, except (F), where paired t test was used. T$_H$, T helper; sc, subcutaneous.

chemokines *Ccl17*, *Ccl22*, *Ccl9*, and *Ccl6* (*40–44*); *Gpr183* [encoding the G protein–coupled receptor EBI2, a critical guidance receptor that positions DCs at the LN follicle border and splenic bridging channels (*45–47*)]; and cell motility regulators such as *Msn* (moesin) and *Cd81* (Fig. 2D). Conversely, biotin$^+$ DCs down-regulated several

genes expressed in anti-inflammatory DCs and/or associated with the induction of T cell tolerance, such as *Tbc1d4*, *Mfge8*, and *Cblb* (*48–50*) (Fig. 2D). Although up-regulation of several of these genes was confirmed at the protein level by flow cytometry (fig. S2D), none of the molecules we tested was alone capable of unequivocally

Fig. 2. Biotin⁺ DCs represent a transcriptionally distinct DC state. (**A**) Clustering of DCs sorted from a tdLN or steady-state iLN. Cells pooled from two steady-state and two tumor-bearing mice from two independent experiments. (**B**) Distribution of steady-state iLN, biotin⁻ tdLN, and biotin⁺ tdLN DCs. (**C**) Proportion of cells in each cluster. (**D**) Expression of genes significantly up-regulated in biotin⁺ cDC1s and cDC2s. (**E**) Violin plots show the most up-regulated gene signatures in biotin⁺ cDC1s and cDC2s. GO, Gene Ontology. (**F**) t-SNE plots showing the distribution of biotin⁻ (left) and biotin⁺ DCs at 10 (center) or 15 (right) d.p.i. in the tdLNs of B16^OT-II–bearing mice. Dotted circles indicate the approximate location of cluster 0. (**G**) Distribution of clusters from Fig. 2A among biotin⁺ and biotin⁻ DCs from 10 and 15 d.p.i. (**H**) Contour plots show the percentage of biotin⁺ DCs in the tdLNs of B16^OT-II tumor-bearing mice at 10 (early) or 15 (late) d.p.i. (**I**) Quantification of data as in (H) (n = 10 or 11 mice per group from four independent experiments; each dot represents one mouse). (**J** and **K**) As in (H) and (I) but in MC-38^OT-II tumor–bearing mice (n = 5 or 7 mice per group, with bilateral tumors; each dot represents one tdLN; data from one experiment). Experiments in (H) to (K) used the Cd40lg^SrtAv1 allele. (**L**) t-SNE plot showing clustering (left) and expression of the LIPSTIC⁺ gene signature (center) among tdLN myeloid cells under control conditions or upon T_reg cell depletion. Right: Expression of the LIPSTIC⁺ signature by cluster. (**M**) Percentage of DCs from control versus T_reg-depleted conditions in cluster 6 versus in all cells. (**N**) Expression of the LIPSTIC⁺ signature in DCs from control or T_reg-depleted mice in cluster 6 among total cDC1s and cDC2s. Data in (L) to (N) are from (13). (C, G, and M) Pearson's chi-square test, (D, E, and N) Wilcoxon signed-rank test, and (I and K) unpaired t test.
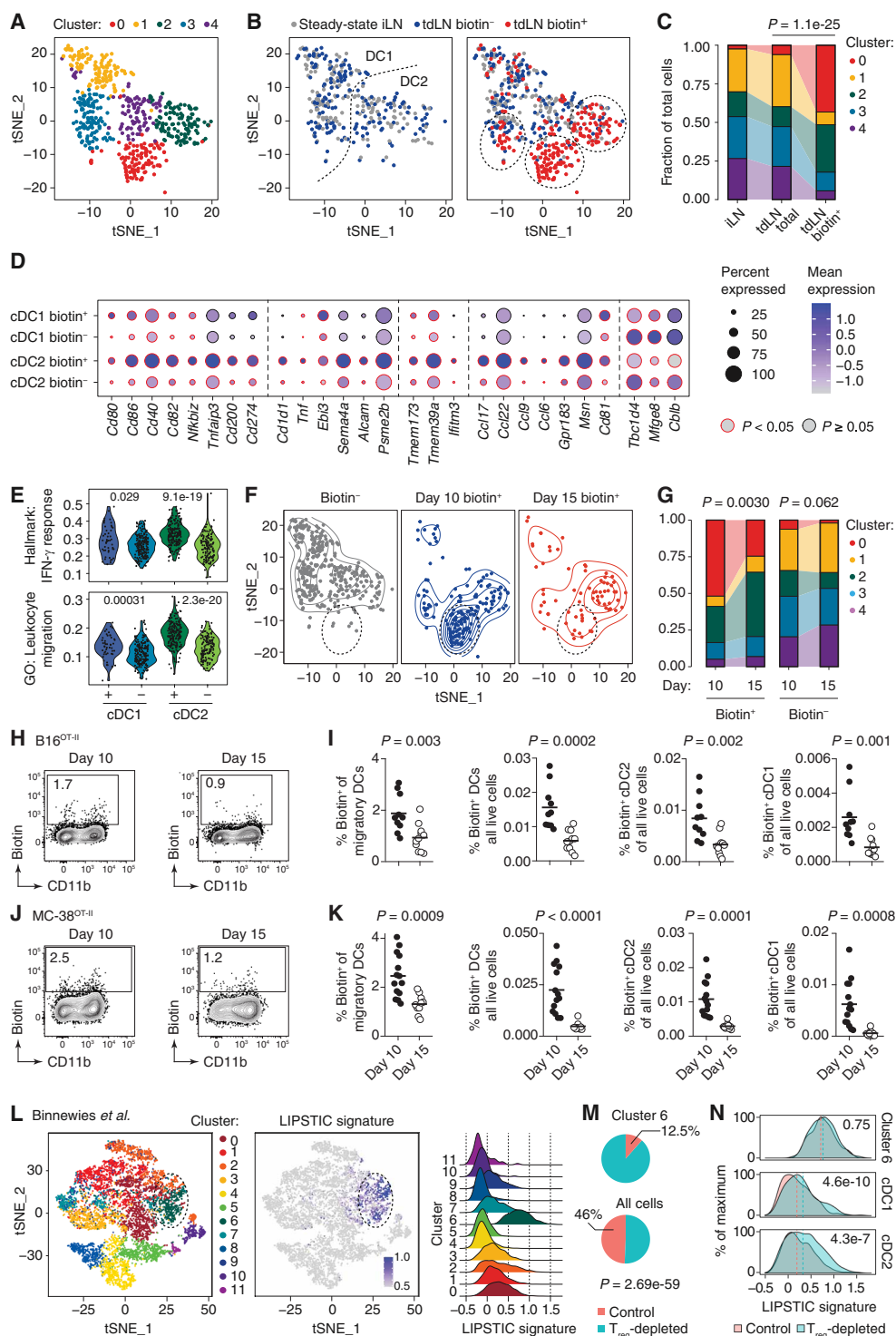
distinguishing between biotin⁺ and biotin⁻ DCs. We confirmed findings pertaining to individual genes at the level of entire gene signatures obtained from the Gene Ontology and Hallmark Molecular Signatures Database (MSigDB) databases (51, 52). Biotin⁺ cDC1s and especially cDC2s showed higher expression of inflammation/activation signatures as well as of signatures related to cell migration, motility, and regulation of the actin cytoskeleton (Fig. 2E, fig. S2E,

and data file S3). Last, although biotin⁺ DCs expressed higher levels of the mRegDC and cDC3 (20, 53) signatures, overlap between our biotin⁺ LIPSTIC signature and these two gene sets was only moderate, indicating that both programs are related but not identical to that of LIPSTIC-labeled DCs (fig. S2, F and G).

LIPSTIC-labeled DCs in the tdLN at day 15 largely lost expression of the signature of cluster 0, the cluster most enriched in biotin⁺

DCs (Fig. 2, F and G), although they by definition interacted with OT-II T cells via the CD40/CD40L axis. Thus, CD40-mediated interaction with T cells is not sufficient to up-regulate the LIPSTIC-related cluster 0 program in DCs. This finding suggested that tumor progression impairs the ability of DCs to prime naïve CD4+ T cells in the tdLN. Flow cytometry of LIPSTIC labeling at early (day 10) and late (day 15) time points confirmed this notion, because labeling of migratory cDC1s and cDC2s fell by roughly one-half between 10 and 15 d.p.i. (Fig. 2, H and I). To extend this observation to a second tumor model, we engineered the MC-38 colon adenocarcinoma cell line (54) to express the OT-II peptide (MC-38^{OT-II}; fig. S1A). As with B16 tumors, LIPSTIC labeling of MC-38^{OT-II} by OT-II T cells also decreased with time, again with comparable reductions in cDC1 and cDC2 populations (Fig. 2, J and K). Thus, DCs that present tumor-derived antigens to CD4+ T cells decrease in numbers and lose their hyperactivated phenotype as the tumor progresses.

To determine whether DCs with a similar hyperactivated phenotype could be detected in tdLNs in the absence of exogenous T cell transfer, we generated a LIPSTIC+ signature consisting of the 224 genes most highly up-regulated in biotin+ compared with biotin− DCs (data file S4). We then applied this signature to a previously published set of single-cell transcriptomes of tdLN myeloid cells obtained at 14 d.p.i. with B16 melanoma, either in control conditions or after depletion of T$_{reg}$ cells using a $Foxp3^{DTR}$ mouse allele. The LIPSTIC signature was expressed predominantly by one group of cells in this dataset (cluster 6), corresponding to cDC2 phenotype DCs (Fig. 2L). Although DCs from control tdLNs were also present, the large majority of cells in this group (87.5%) originated from T$_{reg}$-depleted mice (Fig. 2M). Conversely, comparison of DCs from control and T$_{reg}$-depleted settings showed up-regulation of the LIPSTIC signature in cDC2s and to a lesser extent cDC1s, whereas DCs in cluster 6 expressed this signature equally regardless of whether they originated in control or T$_{reg}$-depleted mice (Fig. 2N). We conclude that DCs with a LIPSTIC-like phenotype can be detected in low numbers in the tdLNs of tumor-bearing mice in the absence of T cell transfer and increase in abundance on depletion of T$_{reg}$ cells.

Together, our data indicate that DCs actively engaged in antigen presentation to CD4+ T cells are in a distinct transcriptional state comprising classic features of DC activation, potentially downstream of T cell help itself, as well as increased expression of locomotion and migration genes. These features suggest that interacting DCs have an enhanced ability to colocalize with T cells in LN regions conducive to T cell priming.

IL-27 produced by tumor antigen–presenting DCs promotes an effective antitumoral response

Among the most highly up-regulated genes in cluster 0 at 10 d.p.i. were $Ebi3$ and $Il27$, which encode for EBI3 and p28—the two subunits of the cytokine interleukin-27 (IL-27; Fig. 3A and fig. S2C). IL-27 is a pleiotropic cytokine that can exert pro- or anti-inflammatory roles depending on the setting (55, 56) and has been shown to either promote or suppress tumor growth in different experimental models (57, 58). To investigate the effects of IL-27 in our setting, we treated mice 9 days after subcutaneous inoculation of B16^{OT-II} cells with either a blocking antibody to p28 or an isotype control. One day later, we adoptively transferred OT-II T cells into tumor-bearing mice and followed the fate of these cells as they were primed in the tdLN and infiltrated the tumor (Fig. 3B). In the tdLN, blocking p28 reduced

the ability of OT-II T cells to express CXCR3 and interferon-γ (IFN-γ), critical mediators of T helper cell 1 effector function (Fig. 3C) (59). In agreement with the role of CXCR3 in promoting effector T cell trafficking to the tumor site (17, 60), p28 blockade reduced OT-II T cell recruitment to the tumor, coinciding with a decrease in production of IFN-γ by this population (Fig. 3D). Parallel experiments using B16^{OVA} showed that anti-p28 treatment also reduced IFN-γ production by OT-I CD8+ T cells in both the tdLN and tumor, although no difference in expression of CXCR3 or tumor infiltration was observed (fig. S3, B and C).

To assess the importance to the antitumoral response of the loss of T cell effector function upon p28 blockade, we used our engineered B16^{mOVA}, which showed delayed growth kinetics in comparison with B16^{OT-II} and was often completely rejected by the host (fig. S1A). Treatment of mice inoculated with B16^{mOVA} with p28 blocking antibody starting at 2 d.p.i. (Fig. 3E) resulted in increased tumor size and weight when compared with control treatment (Fig. 3F). To determine whether IL-27 produced by DCs was required for this antitumor immunity, we inoculated B16^{mOVA} cells into CD11c ($Itgax$)-cre $Il27^{flox/flox}$ mice, in which DCs are deficient in production of IL-27. Although baseline rejection of B16^{mOVA} tumors was less pronounced in control $Il27^{flox/flox}$ mice lacking cre recombinase (possibly because of differences in the mouse housing environment where these experiments were performed), tumor growth was still significantly increased in mice lacking DC production of IL-27 (Fig. 3G) compared with controls. Thus, IL-27 produced by activated DCs is required for full priming of CD4+ T cells and for antitumor immunity in this setting.

CD4+ T cells engage in antigen-specific interactions with APCs in the TME

Recent studies have shown that DCs can influence antitumor immunity locally in the TME through direct interactions with T cells (25). In addition, colocalization of APCs and T cells in the TME in patients with cancer correlates positively with responsiveness to anti–programmed cell death protein 1 (PD-1) immunotherapy (61). However, the extent to which different APC subsets engage and respond to CD4+ T cells under steady-state and immunotherapy conditions is still unclear (24–26). We measured CD40-dependent interactions between T cells and myeloid cells in the TME (rather than the tdLN) by implanting B16^{OTII} tumors into $Cd40^{G5/+}.Cd40lg^{SrtAv2}$ mice, in which all CD40L-expressing endogenous T cells label the CD40-expressing APCs with which they interact (Fig. 4A). At 10 d.p.i., the TME myeloid compartment comprised classical CD11c+MHC-II+ cDCs and Ly6C+MHC-II^{hi} monocytes/monocyte-derived DCs, as well as a large population of F4/80+CD11b+ macrophages (fig. S4A). All three populations expressed MHC-II and CD40 and, thus, had the potential to be labeled by LIPSTIC (fig. S4B); however, labeling was evident only in a minority of classical DCs and Ly6C+MHC-II^{hi} APCs, whereas labeling of MHC-II^{hi}CD40+ macrophages was close to background levels (Fig. 4B). As in the tdLN, the cDC1 and cDC2 subsets were labeled in a ratio mirroring the overall cDC2/cDC1 ratio in the TME (fig. S4C). Biotin+ TME DCs up-regulated the same surface markers as their tdLN counterparts, indicating that T cell–engaged DCs are also in a hyperactivated state in the tumor (Fig. 4C). CD200 up-regulation in the TME was found almost exclusively among biotin+ cDCs and may thus be useful as a marker for T cell–engaged DCs in WT mice (Fig. 4C). Treatment with an anti–MHC-II blocking antibody completely abrogated labeling,
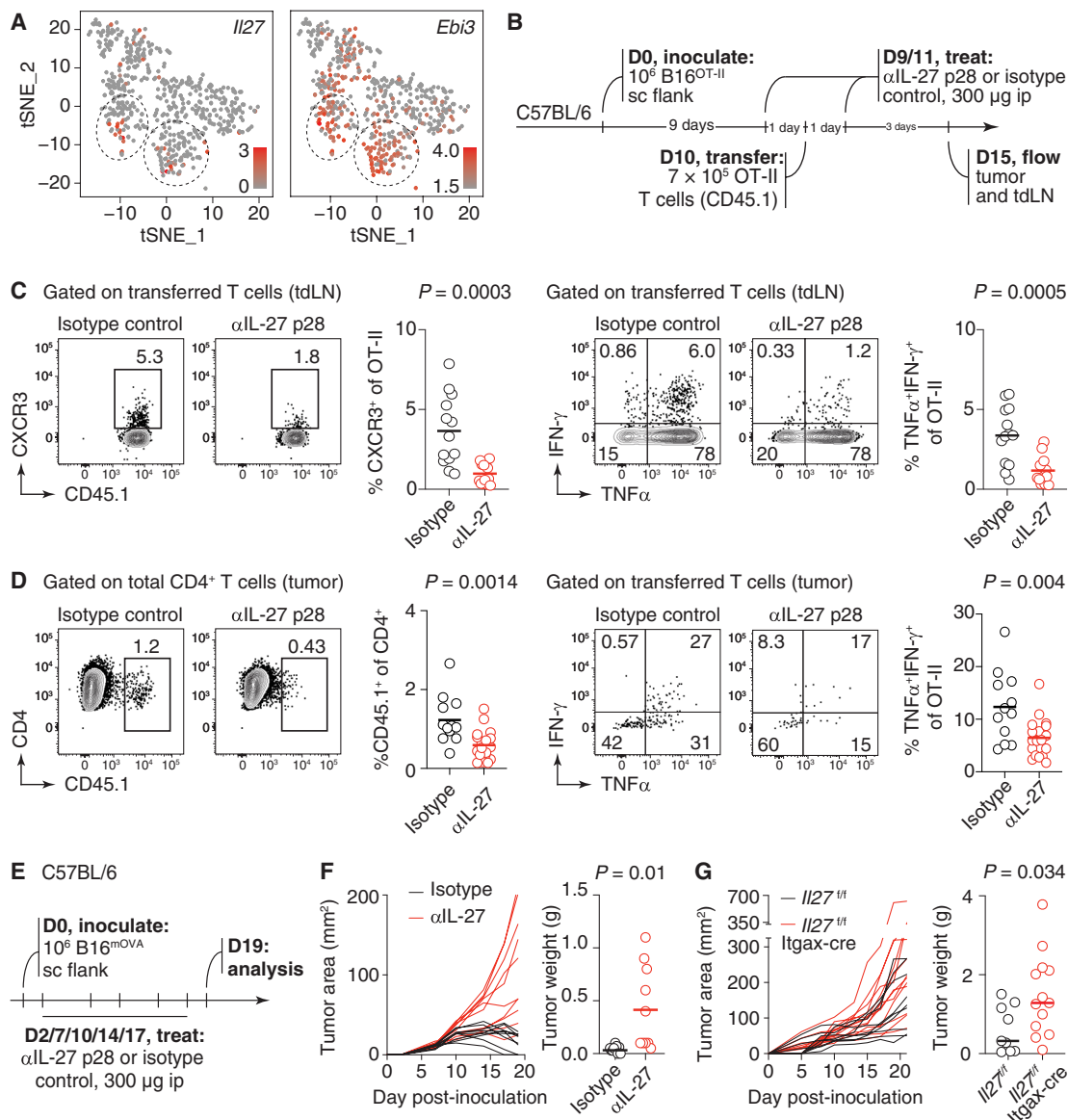
Fig. 3. IL-27 promotes an antitumor CD4+ T cell response and drives antitumor immunity. (**A**) Expression of *Il27* and *Ebi3* in DCs. t-SNE plot as in Fig. 2A. (**B**) Schematic for IL-27 (p28) blocking in mice bearing B16^OT-II tumors. (**C**) Expression of CXCR3+ (left) or tumor necrosis factor–α (TNFα) and IFN-γ (right) among OT-II T cells in tdLNs of isotype or anti-p28–treated mice. Graphs summarize pooled data from 13 mice per group from two independent experiments. (**D**) Percentage of OT-II cells among all CD4+ T cells (left) and expression of TNFα and IFN-γ among OT-II T cells (right) in the tumors of isotype or anti-p28–treated mice. Graphs summarize pooled data from 12 and 18 mice per group from two independent experiments. (**E**) Schematic for IL-27 (p28) blocking in mice bearing B16^mOVA tumors. (**F**) Tumor growth curves and tumor weights for isotype control and anti-p28–treated groups (*n* = 9 or 10 mice per group from one experiment). (**G**) Tumor growth curves and tumor weights for *Il27^f/f* (control) and *Il27^f/f* Itgax-Cre groups. Data are from 9 control and 13 *Il27^f/f* Itgax-Cre mice pooled from four independent experiments. *P* values are for unpaired *t* test. ip, intraperitoneal.

suggesting that T cell–APC interactions in the TME are antigen specific (Fig. 4D). This was corroborated by coculture experiments, which showed that biotin+ DCs from mice carrying B16^OT-II or B16^mOVA tumors were more potent drivers of naïve OT-II and OT-I T cell proliferation, respectively, than biotin− DCs from the same tumors (Fig. 4E), although TME-resident biotin− DCs were able to drive more substantial proliferation than their counterparts in the tdLN (Fig. 1H). Although most APCs were loaded with tumor-derived antigens (as estimated by their GFP fluorescence), there was

little if any correlation between GFP fluorescence and LIPSTIC labeling (fig. S4D), indicating that these two measures cannot substitute for each other. We concluded that tumor-infiltrating CD4+ T cells interact with TME DCs in an antigen-specific manner and that this interaction is associated with enhanced DC activation.

To better understand the nature of the interactions between myeloid cells and CD4+ T cells in the TME, we used droplet-based scRNA-seq combined with an antibiotin hashtag oligo (HTO)–barcoded antibody (*62*). We first performed LIPSTIC labeling in
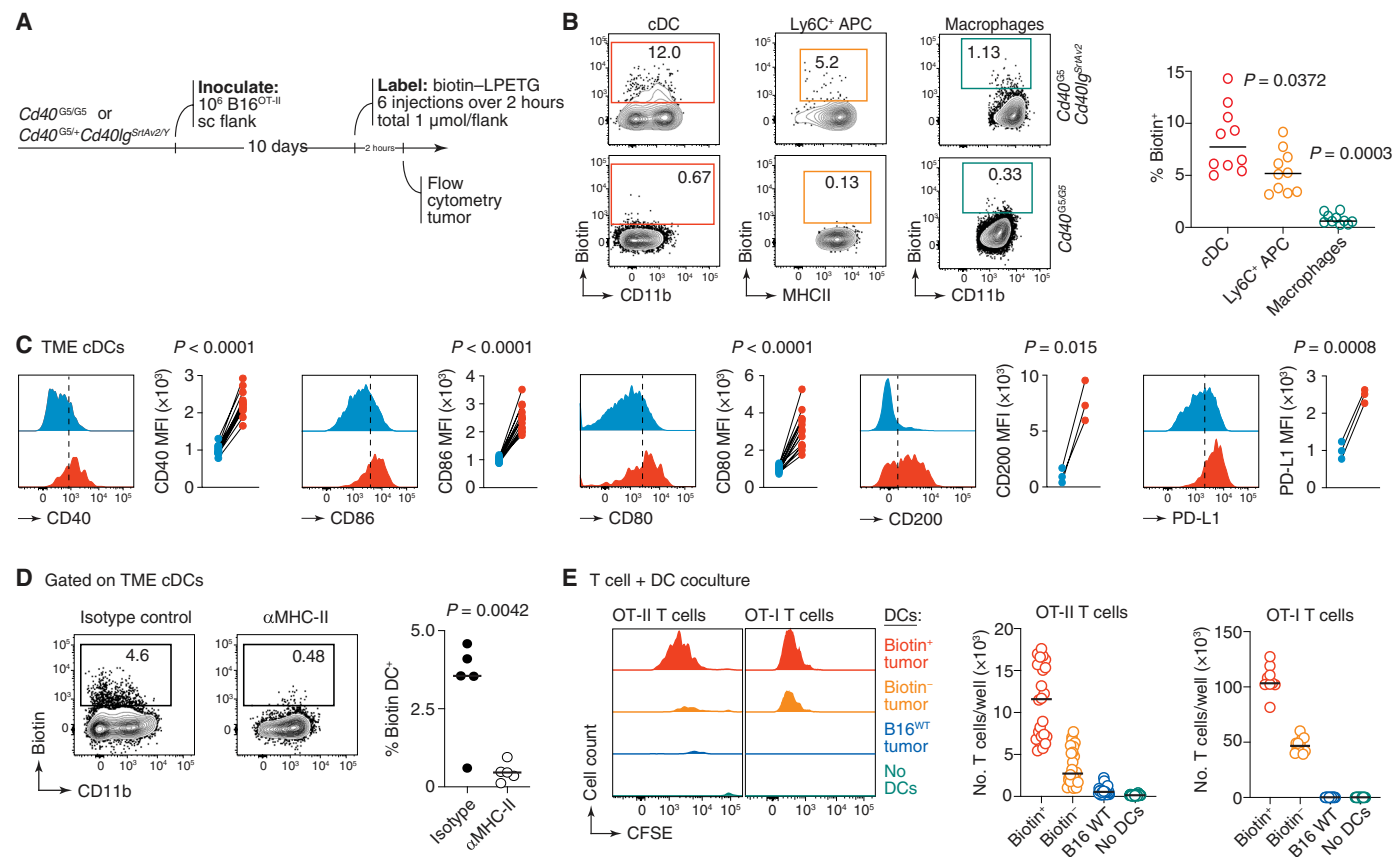
Fig. 4. Using LIPSTIC to identify APCs in the tumor. (**A**) Experimental setup for (B) to (D). (**B**) Percentage of labeled APCs in ($Cd40^{G5/+}Cd40lg^{SrtAv2}$) mice bearing B16^{OTII} tumors (left) and quantification of data (right) ($n = 10$ mice from four independent experiments). $Cd40^{G5/G5}$ mice were used as a baseline for biotin. (**C**) Mean fluorescent intensity (MFI) normalized to the MFI of biotin$^-$ DCs for the indicated molecules. Biotin$^+$ (red) and biotin$^-$ (blue) DCs in the TME (for CD40, CD86, and CD80, $n = 14$ mice from four experiments; for CD200 and PD-L1, $n = 3$ mice from one experiment). (**D**) Experimental setup as in (A) except that anti–MHC-II or isotype control antibodies were injected 2 hours before substrate injection intratumorally (200 μg). Left: Contour plots show percentage of labeled DCs. Right: Quantification of labeled DCs ($n = 5$ mice from two independent experiments). (**E**) Proliferation of OT-II and OT-I T cells in vitro after 96 hours of coculture with DCs derived from mice carrying B16^{OT-II} or B16^{mOVA} tumors, respectively, (left) and quantification of T cells per well at the end of the culture period (right). For (E), tumors were pooled from $n = 5$ or 9 mice from two independent experiments. Each dot represents one culture well. P values are for one-way ANOVA (B), paired t test (C), and unpaired t test (D).

B16^{OT-II}–bearing mice as in Fig. 4A, except that animals were treated with an isotype control antibody for later comparison with anti–CTLA-4–treated mice (described below). We then sorted TME myeloid cells both as total cells (unenriched) or as a biotin$^+$ fraction (enriched) (fig. S5A) at 15 d.p.i. and performed scRNA-seq using the 10X Genomics Chromium platform. Myeloid cells clustered into monocytes/macrophages (Mos/MΦs), cDC1s, cDC2s, and a series of clusters of activated DCs expressing the mRegDC/DC3 signature (20, 53), which we combined into the mRegDC1 and mRegDC2 clusters on the basis of their proximity to cDC1s and cDC2s and their expression of subtype-specific gene signatures (Fig. 5A; fig. S5, B to D; and data file S5). Whereas LIPSTIC labeling was noted in a small subset of Mos/MΦs, it was most pronounced in the two mRegDC clusters (Fig. 5B). Separating cells on the basis of whether they came from the LIPSTIC-enriched or LIPSTIC-unenriched samples showed that the large size of the Mo/MΦ and mRegDC clusters in the total pool was in part due to the higher abundance of cells with this phenotype among the biotin$^+$ population (fig. S5E). Biotin$^+$ cells up-regulated genes important for antigen presentation (*Psme2*, *Serpinb9*, *H2-DMb2*, and *H2-DMa*) (36, 63, 64) and DC maturation

(*Traf1* and *Stat1*) (65, 66), costimulatory molecules (*Cd40*, *Cd1d1*, *Cd70*, *Cd200*, and *Cd48*) (67), and chemokines and cytokines important for T cell–mediated antitumor immunity (*Cxcl9*, *Cxcl16*, and *Ebi3*) (17, 58, 68, 69) (data file S5). Thus, interaction with T cells is associated with an enhanced activation state among myeloid cells in the TME, as it was in the tdLN. Accordingly, all major DC clusters up-regulated the genes included in the tdLN_LIPSTIC$^+$ signature (Fig. 5C), which overlapped substantially, if less than fully, with the corresponding TME_LIPSTIC$^+$ signature obtained by comparing biotin$^+$ and biotin$^-$ TME DCs (fig. S5F). Thus, as in the tdLN, myeloid cell interaction with T cells in the TME was associated with an enhanced activation state. Plotting trajectories from cDC1 and cDC2 to their adjacent mRegDC subclusters showed that the onset of LIPSTIC labeling either slightly preceded (cDC1) or closely coincided with (cDC2) up-regulation of the mRegDC signature in pseudotime, suggesting that CD40L-mediated T cell help may play a role in establishing the mRegDC phenotype (Fig. 5, E and F). Nevertheless, plotting the expression of the mRegDC signature (20) against that of CD40 target genes (29) revealed two populations: an mRegDC × CD40 diagonal, comprising mostly cDC1s and cDC2s, where expression
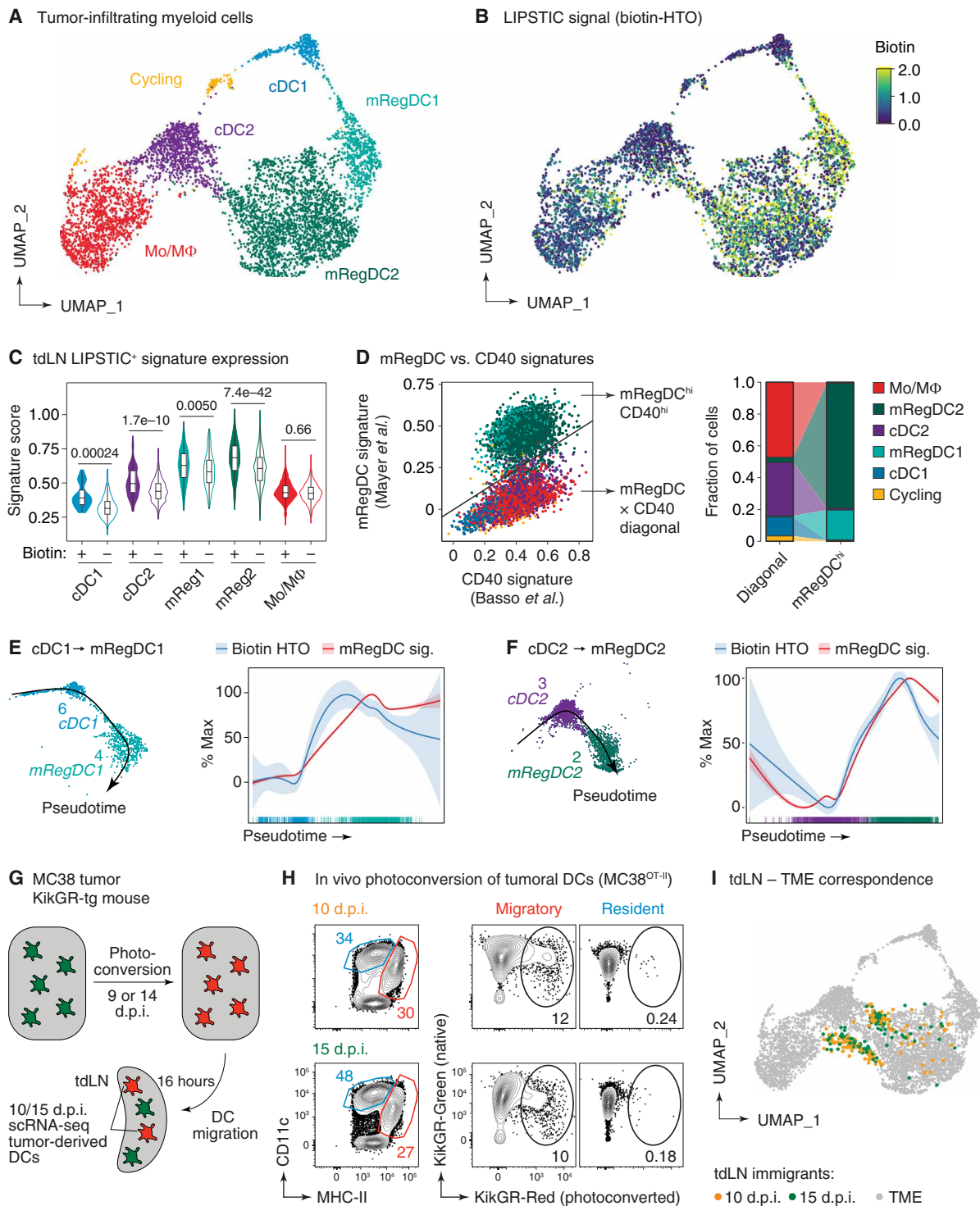
Fig. 5. Single-cell interaction-based transcriptomics of APCs in the TME. (**A**) Uniform manifold approximation and projection (UMAP) plot showing manually annotated clustering of MHC-II^{+} myeloid cells sorted from the TME at 15 days after tumor inoculation. See fig. S5B for unsupervised clustering. (**B**) Distribution of LIPSTIC signal (antibiotin DNA hashtag labeling) in the same cells in log-normalized counts. (**C**) Expression of the tdLN_LIPSTIC[+] signature in biotin[+] and biotin^{−} cells in the indicated populations. P value is for Wilcoxon signed-rank test. (**D**) Scatterplot showing the expression of CD40 mRegDC gene signatures for the indicated populations of cells (left) and quantification of indicated populations in the mRegDC × CD40 diagonal and mRegDC^{hi} CD40^{hi} clusters. (**E**) Pseudotime trajectory showing the transition from cDC1s to mRegDC1s (left) and biotin acquisition and expression of the mRegDC program along that trajectory (right). (**F**) As in (E) but for cDC2s. Results in (A) to (F) are for four mice pooled in one experiment. (**G**) Schematic depicting the tumor photoconversion experiment. (**H**) Percentage of photoconverted migratory and resident DCs in the tdLN at 10 (early, top) and 15 (late, bottom) d.p.i. with (results are representative of $n = 6$ mice per group from one experiment). (**I**) UMAP showing correspondence between tumor APCs and photoconverted DCs arriving at the tdLN, using the MapQuery function of Seurat.

of both signatures correlated positively, and an mRegDC^{hi}CD40^{hi} population comprising cells classified as bona fide mRegDCs in our clustering (Fig. 5D). Thus, although mRegDCs showed signs of CD40-mediated activation, CD40 target genes comprised only part of the full mRegDC program, suggesting that other factors, such as antigenic uptake or exposure to cytokines (20), may also be involved in the acquisition of a full mRegDC state.

To gain insight into which of these TME DC populations was most likely to migrate to the tdLN, we used an in situ photoconversion protocol similar to one previously described in the literature (70) to directly measure the state of DCs arriving from the tumor to the tdLN. We injected mice ubiquitously expressing the photoconvertible *Kikume* green-to-red (KikGR) protein (71, 72) with MC-38^{OT-II} cells, which allow efficient photoactivation because of the lack of the dark pigmentation characteristic of B16 tumors (Fig. 5G). Photoactivation of tumors under a 415-nm light-emitting diode (LED) source led to the accumulation of photoconverted migratory, but not resident, DCs in the tdLN as early as 16 hours after photoconversion (Fig. 5H), allowing us to isolate DCs immediately after they arrived at the tdLN from the tumor. We performed scRNA-seq profiling of photoconverted DCs sorted from the tdLN at 10 and 15 d.p.i. (i.e., 16 hours after photoactivation at 9 and 14 d.p.i., respectively; Fig. 5G) and mapped photoconverted tdLN DCs to their closest neighbors in the TME dataset (Fig. 5I). We found that DCs arriving at the tdLN were most closely related to cells transitioning between the cDC2 and mRegDC2 phenotypes, with fewer cells scattered in the more-differentiated mRegDC2 clusters. Plotting the expression of mRegDC and CD40 signatures for photoactivated TME emigrants (fig. S5G) and for all tdLN DCs analyzed in the LIPSTIC experiment (Fig. 2, A to G) showed that they lay mostly on the mRegDC × CD40 diagonal, with no evidence of an additional mRegDC^{hi}CD40^{hi} population as found for TME-resident cells (compare Fig. 5D and fig. S5G). These findings are consistent with a model in which cDC2s exit the TME to migrate to the tdLN before fully acquiring the mRegDC signature (73).

Checkpoint inhibition increases CD40-CD40L interactions in the TME

Checkpoint inhibitor–blocking antibodies, such as those targeting CTLA-4 and PD-1, strongly promote antitumoral T cell responses and, as such, have become the key component of tumor immunotherapy. Mechanistically, they are thought to work not only by enhancing the effectiveness of T cell priming in the tdLN but also by reviving exhausted T cells in the TME (74, 75). We first sought to determine whether we could rescue late DC dysfunction in the tdLN (Fig. 2, F to K) using the same experimental setup but in the context of checkpoint blockade (Fig. 6A). Treatment of tumor-bearing mice with anti–CTLA-4 led to a marked increase in the number of labeled DCs in the tdLN (Fig. 6B) while skewing their composition toward the CD11b$^+$ cDC2 subset (Fig. 6C). To search for similar effects in the TME, we treated tumor-bearing *Cd40*$^{G5/+}$.*Cd40lg*^{SrtAv2} mice with three injections of anti–CTLA-4 or anti–PD-1 blocking antibodies (or their respective isotype controls) at days 5, 7, and 9 after tumor implantation and performed LIPSTIC labeling and analysis the following day (Fig. 6D). Treatment increased the number of biotin$^+$ APCs (Fig. 6, E and F), an effect that was evident among both classical DCs and Ly6C$^+$MHC-II^{hi} APCs. PD-1 blockade led to a less-pronounced increase among DCs and possibly also

Ly6C$^+$MHC-II^{hi} APCs (fig. S6A), leading us to focus our subsequent analysis on anti–CTLA-4 treatment.

Analysis of TME populations by scRNA-seq showed that anti–CTLA-4 treatment increased biotin labeling not only among cDC2s (which showed the largest fold change in biotin levels) and mRegDCs (which, given their large numbers, accounted for most of the increase in biotin$^+$ DCs upon treatment) but also in the Mo/MΦ cluster (Fig. 6, G and H). Most subsets significantly up-regulated the expression of the tdLN_LIPSTIC$^+$ signature upon treatment, an increase that was notably more pronounced in cDC populations than in their mRegDC counterparts (Fig. 6I). cDC2s additionally upregulated CD40 target genes (fig. S6B). This pattern suggests that anti–CTLA-4 treatment broadens the acquisition of a hyperactivated state to a larger DC population but does not result in the establishment of a distinct, checkpoint blockade–specific DC state. Consistent with this, an analysis of differential gene expression comparing only the biotin$^+$ TME DCs from anti–CTLA-4–and isotype control–treated mice revealed few significant differences (Fig. 6J). Thus, checkpoint blockade with anti–CTLA-4 appears to amplify the extent to which T cells interact with APCs, especially cDC2s, in the TME. This interaction, in turn, leads to increased expression of both tdLN and TME LIPSTIC signatures, especially in less-differentiated DC subsets.

DISCUSSION

A challenge in studying the priming capabilities of DCs has been the heterogeneity in their phenotypes, even in canonical DC populations (48, 76). Whereas the literature is plentiful in associations between the broader populations of DCs (such as cDC1s and cDC2s or migratory and resident DCs) and the priming of specific types of T cell responses (12, 77), studies that characterize the individual DCs directly engaged in T cell priming are rare (78). LIPSTIC provides an easy and highly quantitative method to identify and profile T cell–engaged DCs at the individual cell level. As such, LIPSTIC provides a degree of specificity to DC research analogous to that afforded to B and T cell studies by antigen tetramers (79, 80).

Our LIPSTIC data revealed that the fraction of all tdLN DCs that actively present antigen to CD4$^+$ T cells in response to a subcutaneously implanted tumor was relatively small, on the order of 5 to 15% of the DCs in the LN even at the early time point peak. These DCs were almost entirely of the CD11c^{low}MHC-II^{hi} migratory phenotype and were not enriched in cDC1s or cDC2s when compared with the entire LN DC population. In coculture experiments, tdLN biotin$^+$ DCs were exclusively able to drive the proliferation of both CD4$^+$ and CD8$^+$ T cells. This suggests that the DCs that prime CD8$^+$ T cells responses in vivo are included in the DC population labeled by CD4$^+$ T cells, indicating substantial overlap between these populations. Thus, CD40L LIPSTIC is unlikely to be missing any major population of DCs capable of presenting antigen exclusively to CD8$^+$ T cells in the tdLN. Further work using CD8$^+$ T cell LIPSTIC (62) will be required to assess whether any minor populations of DCs exist that are exclusively tasked with priming CD8$^+$ T cells. Our findings contribute to a series of active discussions in the field regarding the numbers and population-level phenotypes of the DCs that prime the antitumoral T cell response (6, 7, 12, 13, 20, 81).

A potential limitation of LIPSTIC is that it identifies only DCs that engage T cells through the CD40L-CD40 pathway. Most if not
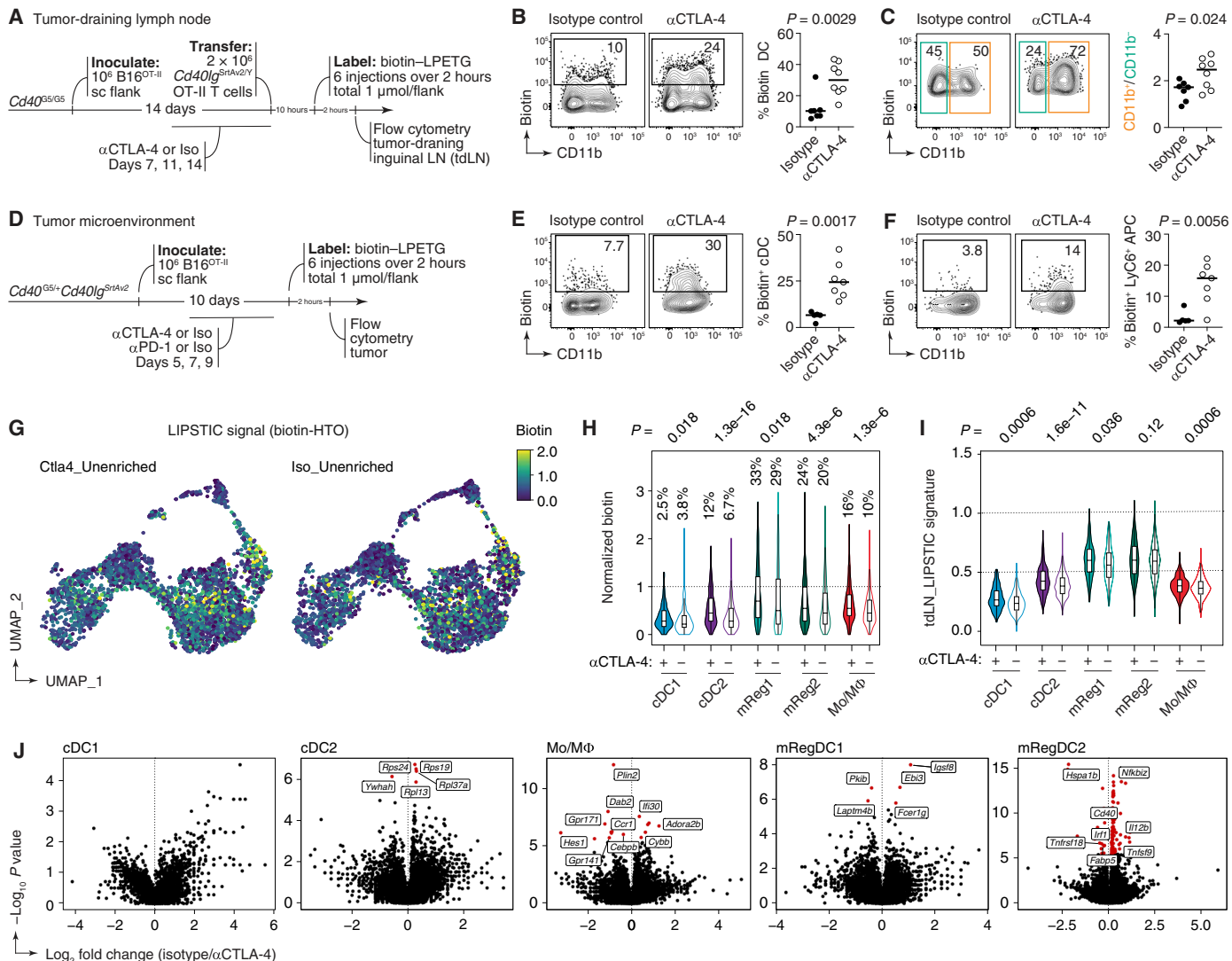
Fig. 6. Checkpoint blockade amplifies the CD40-CD40L interaction axis in the tdLN and TME. (**A**) Experimental setup for (B) and (C). (**B**) Contour plot and quantification of biotin+ DCs in the tdLN in the indicated groups. ($n = 7$ for isotype control and $n = 8$ for CTLA-4 from two independent experiments). (**C**) Contour plot and quantification of CD11b+ and CD11b− DCs among biotin+ cells. (**D**) Experimental setup for (E) and (F). (**E**) Contour plot and quantification of biotin+ DCs in the TME in the indicated groups. ($n = 5$ for isotype control and $n = 7$ for anti–CTLA-4, from two independent experiments). (**F**) Contour plot and quantification of biotin+ Ly6C+ APCs in the TME in the indicated groups. For (B), (C), (E), and (F), P values were calculated using an unpaired t test. (**G**) UMAP plot showing the distribution of LIPSTIC signal (anti-biotin DNA hashtag labeling, in log-normalized counts) in anti–CTLA-4 versus isotype control–treated groups ($n = 4$ for control and $n = 3$ for anti–CTLA-4 pooled in one experiment). (**H**) Violin plots showing antibiotin DNA hashtag labeling (LIPSTIC signal) in the indicated populations in anti–CTLA-4 and isotype control groups. Percentage of biotin+ cells is given for each violin. (**I**) Violin plots showing expression of the tdLN_LIPSTIC+ signature in anti–CTLA-4–and isotype control–treated groups in the indicated populations. For (H) and (I), P values were calculated using Wilcoxon signed–rank test. (**J**) Volcano plots showing differentially expressed genes between biotin+ APCs from isotype control–and anti–CTLA-4–treated mice. Statistically significant genes are colored in red.

all conventional CD4+ T cells are thought to express CD40L even in their naïve state (*82*) and to up-regulate its expression upon antigen-driven activation (*83*). Conversely, most DCs express CD40, although its expression by resident DCs is generally lower than by DCs with a migratory phenotype (*84*). Nevertheless, because the CD40L-CD40 axis is critical for DC activation and licensing for cross-presentation (*85–88*), CD40L LIPSTIC is likely to identify most or all DCs that are potent presenters of immunogenic tumor antigens. This notion is supported by our miniaturized DC culture assays, in which LIPSTIC-negative DCs were unable to induce

proliferation of CD4+ or CD8+ T cells above background levels, indicating that most antigen-presenting capability is concentrated in the LIPTSIC+ DC population.

Interaction-based transcriptional profiling of LIPSTIC-labeled cells showed that the DCs that present tumor-derived antigens to naïve CD4+ T cells in vivo expressed a distinct transcriptional profile that separated them from other DCs in the tdLN. Total DCs from tdLN were indistinguishable transcriptionally from DCs obtained from a naïve iLN, implying that this population of DCs, or at least their prominent role in driving T cell activation and proliferation,

would be difficult to identify without LIPSTIC. The ability to drive T cell responses was associated with up-regulation of multiple genes important for DC activation and antigen presentation. These included classic DC maturation markers, such as *Cd80*, *Cd86*, and *Cd40* itself (*89*), indicative of partial overlap with the canonical "mature DC" phenotype (*90*). However, LIPSTIC-labeled DCs also up-regulated multiple genes and signatures associated with cell migration, adhesion, and T cell chemotaxis (*91*). Thus, the ability of DCs to access specific microanatomical compartments and to recruit T cells to these areas, previously shown to be functionally important for T cell responses (*45–47*, *92*), is one of the defining characteristics of the DCs capable of engaging T cells in vivo. Intersecting our transcriptional data with a much larger scRNA-seq dataset of tdLN myeloid cells (*13*) revealed a cluster of DCs with strong expression of the tdLN_LIPSTIC[+] signature. A small fraction of this cluster represented DCs found in the tdLN under control nonmanipulated conditions, indicating that the tdLN_LIPSTIC[+] transcriptional state is not a product of our specific setup (e.g., of the adoptive transfer of a relatively large number of tumor antigen–specific T cells). However, the large majority of cells in this cluster consisted of DCs that appeared upon ablation of T_{reg} cells [using a diphtheria toxin receptor (DTR) transgene]. These findings suggest that one of the effects of T_{reg} cells, possibly potentiated in the TME, is to prevent DCs from acquiring a LIPSTIC[+]-like state. The cytokine IL-27 was among the most up-regulated gene products in biotin[+] DCs. IL-27 is an especially pleiotropic cytokine, which has been shown to prime both tolerogenic and immunogenic T cell responses under different conditions (*55–58*, *69*, *93–96*). In our settings, IL-27 produced by DCs was essential for priming IFN-γ production by tumor-specific CD4^{+} and CD8^{+} T cells, recruitment of effector T cells to the tumor site, and control of tumor growth. This result agrees with previous reports in the literature and disagrees with others under similar settings (*57*, *58*). The reasons for these discrepancies remain unclear and merit further investigation.

In addition to their functions in the tdLN, myeloid cells interact with T cells in the TME, shaping antitumor responses locally (*6*, *24*, *25*). Quantifying the relative contribution of various APCs to CD4^{+} T cell stimulation in the TME is challenging because of the vast heterogeneity of the myeloid compartment in tumors (*6*, *24*, *25*, *97*). Our data show that DCs and, to a lesser extent, Ly6C^{+} APCs were the primary populations interacting with CD4^{+} T cells in the TME. Despite high CD40 and MHC-II expression, macrophages engaged minimally with T cells, indicating that factors beyond the expression levels of these molecules influence APC–T cell interactions in the tumor. However, our examination of APC–T cell interactions in the TME was restricted to steady-state and checkpoint blockade conditions—scenarios in which CD40-mediated interactions between APCs and T cells were heavily dominated by mRegDC2s. Future studies will be needed to address the extent to which other cancer treatments such as chemotherapy, radiotherapy, various Toll-like receptor and nod-like receptor agonist treatments, or metabolic interventions can shift interactions toward macrophages or other myeloid populations that can up-regulate CD40 (*98*).

The ability of DCs to interact with T cells in the TME correlated with the expression of classical activation markers, such as *Cd80*, *Cd86*, and *Cd40*, as well as with the expression of the tdLN-derived LIPSTIC[+] signature. Thus, DCs that engage with T cells in the TME are in a hyperactivated state similar to that found among interactors in the tdLN. Our scRNA-seq data showed that DC labeling correlated strongly with (and possibly preceded in time) expression of the mRegDC program in both the cDC1 and cDC2 subsets. This suggests the possibility that, in addition to antigenic capture and IFN-γ signaling (*20*), the mRegDC state may be partially induced by CD40L-mediated T cell help. Additional work will be required to strictly determine whether T cell help drives the mRegDC state or, conversely, whether it is the acquisition of the mRegDC state that poises DCs to engage with CD4^{+} T cells. When we overlaid the scRNA-seq data from photoconverted DCs to our broader 10X dataset, we observed that photoconverted DCs, which emigrated from the tumor to the tdLN, did not fall into the fully differentiated mRegDC cluster present in TME but rather resembled less mature cDC2s. This suggests the existence of additional signals that trigger the exit of DCs from the TME to the tdLN before their full maturation. Speculatively, help provided by CD4^{+} T cells to DCs early after their arrival to the TME may drive DC migration to the tdLN, whereas DCs that remain in the TME may acquire the fully differentiated mRegDC phenotype.

Checkpoint inhibitors have revolutionized cancer therapy, yet the mechanisms underlying their action are not fully resolved (*74*, *99*). Our findings corroborate a previous study indicating that CTLA-4 treatment increases cDC2 migration to the tdLN (*13*). Furthermore, we observed that the amount of interaction between CD4^{+} T cells and DCs is markedly enhanced by checkpoint inhibitors in both the tdLN and the tumor itself. The most significant increase in expression of tdLN_LIPSTIC[+] signature genes upon anti–CTLA-4 treatment was found among the cDC2 and cDC1 subsets, suggesting that checkpoint blockade accelerates the acquisition of a hyperactivated state in tumor DCs. In addition, we observed a significant increase in the CD40 signature exclusively in cDC2s. These results suggest that CTLA-4 blockade may exert its effects in part by promoting the interaction of CD4^{+} T cells with incompletely matured cDC2s in the TME, triggering their activation and migration to the tdLN. This effect can be aided by increased T cell–cDC interactions in the tdLN, as well as by T cell–mRegDC interactions directly in the TME.

In conclusion, LIPSTIC allowed us to identify the individual DCs capable of presenting tumor-derived antigens to CD4^{+} T cells in tdLNs and engaging with these cells in the TME and to define transcriptional programs associated with these interactions at both sites. The in vivo DC activation signature identified in this work has the potential to be exploited practically to improve responses to tumor antigens by therapeutic targeting of DCs or their products. In addition, we expect that the LIPSTIC interaction-based transcriptomic platform laid out in this study will be useful for immunologists wishing to identify the DCs that prime CD4^{+} T cell responses in various settings.

MATERIALS AND METHODS
Study design
DCs have the unique ability to transport tumor-associated antigens to tdLNs, where they prime naïve tumor-specific T cells. In addition, they engage with effector T cells in the TME, contributing to antitumor immunity. Despite the importance of DCs in mediating the antitumor immune response, the physical identification of antigen-presenting DCs in vivo has been challenging. To address this gap, we aimed to identify APCs at the single-cell level in both tdLNs and the TME using LIPSTIC. We profiled these cells using interaction-based

single-cell transcriptomics and characterized interaction dynamics between APCs and T cells at the steady state and upon checkpoint blockade.

Mice

Cd40^{G5} mice were generated as previously described (*28*) and were maintained in our laboratory. Two versions of *Cd40lg*^{SrtA} mice were used, the original conditional version (*28*) (which we refer to as *Cd40lg*^{SrtAv1}) and a constitutive *Cd40lg*^{SrtAv2} version (developed as described below). For intratumoral experiments, we generated *Cd40*$^{G5/+}$.*Cd40lg*^{SrtAv2} mice by crossing *Cd40*^{G5} with constitutive *Cd40lg*^{SrtAv2} (this cross is available from the Jackson Laboratory, strain #037113). Unless indicated in the figure legend, all experiments were done using the constitutive version. C57BL6/J, CD45.1 (B6.SJL Ptprca), *H2*$^{-/-}$ (*100*), CD4-Cre–transgenic (*101*), and OT-I T cell receptor (TCR)–transgenic (*102*) mice were purchased from the Jackson Laboratory (strains 000664, 002014, 003584, 022071, and 0003831, respectively). OT-II TCR–transgenic mice (Y chromosome version) (*103*) were bred and maintained in our laboratory. *Il27*^{flox} (*69*) and Itgax-cre (*104*) mice were bred and maintained at the University of California, San Diego (UCSD). CAG-KikGR–transgenic mice (*71*) were a gift from A. Hadjantonakis (Memorial Sloan Kettering Cancer Center). CAG-KikGR–transgenic mice were backcrossed to the C57BL6 background for at least 10 generations at Rockefeller University. All mice were housed in specific pathogen–free conditions, in accordance with institutional guidelines and ethical regulations. All protocols were approved by the Rockefeller University or UCSD Institutional Animal Care and Use Committees. Male and female mice aged 5 to 12 weeks were used in all experiments.

Generation of Cd40lg^{SrtAv2} mice

Cd40lg^{SrtAv2} mice were generated in our laboratory using the EASI-CRISPR method (*105*). Cas9-crRNA-tracrRNA complexes targeting the last exon of the *Cd40lg* locus (GAGTTGGCTTCTCATCTTT) were microinjected along with single-stranded DNA templates encoding a C-terminal SrtA fusion flanked by 200-bp homology arms into the pronuclei of fertilized C57BL6 embryos, which were then implanted into pseudopregnant foster dams. Founder mice were backcrossed to WT C57BL6 mice for at least five generations to reduce the probability of transmitting CRISPR-induced off-target mutations.

Generation of transgenic tumor lines

Constructs were cloned into the pMP71 vector (*106*), which was modified to express a fluorescent reporter [enhanced GFP (eGFP)] followed by a sequence encoding amino acids 323 to 339 of chicken OVA (eGFP-OT-II) or the *Thosea asigna* virus self-cleaving 2A peptide (T2A) (*107*) followed by the full-length OVA protein (eGFP-OVA). Retroviruses were produced in human embryonic kidney (HEK) 293 cells using CaCl$_2$ transfection. Gag-Pol and VSV plasmids were used for virus packaging. The virus-containing supernatant was harvested 48 hours after transfection, spun down at 252*g* for 5 min, and filtered through a 0.45-μm filter. The B16-OT-II, B16-OVA, melanoma cell line, and the MC38-OT-II colon adenocarcinoma cell line were produced by retroviral transduction with eGFP-OT-II or eGFP-OVA constructs. Briefly, the viral supernatant from HEK-293 cells was added to B16 or MC-38 cells with polybrene (5 mg/ml; Sigma-Aldrich, H9268), and cells were spun down at 800*g* for 90 min at 30°. The viral supernatant was replaced with regular medium

12 hours after transfection; 60 hours after transfection, eGFP$^+$ cells were sorted using a FACSAria II, expanded, and frozen in liquid nitrogen.

Murine tumor models

All tumor cell lines were grown in Dulbecco's modified Eagle medium supplemented with 1% L-glutamine and 1% penicillin/streptomycin. On the day of tumor injection, tumor cells were trypsinized with TrypLE express, washed twice, and resuspended in sterile phosphate-buffered saline (PBS). Mice were anesthetized and shaved on one or both flanks, and one million tumor cells were injected in 50 μl of PBS subcutaneously (unilaterally or bilaterally) at a site adjacent to the iLN. Tumor growth was assessed two or three times per week by caliper measurements. Tumor area was calculated by multiplying tumor length by tumor width.

Adoptive cell transfer

To isolate CD4$^+$ or CD8$^+$ T cells, spleens were forced through 70-μm filters, red blood cells were lysed with ammonium-chloride-potassium (ACK) lysing buffer (Lonza), and CD4$^+$ or CD8$^+$ T cells were isolated using CD4$^+$ or CD8$^+$ T cell isolation kits (Miltenyi Biotec) as described in the manufacturer's protocols. Purified cells were injected intravenously in 100 μl of PBS.

LIPSTIC in vivo

Biotin-aminohexanoic acid-LPETGS, C-terminal amide, 95% purity (biotin-LPTEG) was purchased from LifeTein (custom synthesis), and stock solutions were prepared in PBS at 20 mM. For LIPSTIC labeling in vivo, biotin-LPETG was injected subcutaneously into the flank (shaved area proximal to tumor and iLN); 50 μl of 20 mM substrate dissolved in PBS (equivalent to 1 μM per injection) was injected a total of six times (6 μM total) 20 min apart, and iLNs were collected 20 min after the last injection, as described previously (*28*). Mice were briefly anaesthetized with isoflurane before each injection. For labeling intratumoral APC–T cell interactions, everything was done as above except that substrate (same amount) was injected intratumorally.

Antibody treatment

For IL-27 blocking experiments, animals were injected intraperitoneally with 300 μg of p28 blocking antibody clone (BioXCell, MM27.7B1) or isotype control clone (BioXCell, C1.18.4). The regimen for each experiment is described in the corresponding figure legend. For CD40L-blockade experiments, mice were injected intravenously with 200 μg of CD40L blocking antibody (clone MR-1, BioXCell) 2 hours before the first injection of substrate. For anti–CTLA-4 treatment, animals were injected as shown in the figure with 200 μg of clone 9H10 (BioXCell) or corresponding isotype control Syrian hamster immunoglobulin G (IgG; BioXCell). For anti–PD-1 treatment, animals were injected as shown in the figure with 200 μg of clone RMP1-14 (BioXCell) or corresponding isotype control rat IgG2a clone 2A3 (BioXCell). For the MHC-II blocking experiment, mice were injected intratumorally with 200 μg of anti–MHC-II blocking antibody (I-A/I-E; clone M5/114, BioXCell) 2 hours before the first substrate administration or isotype rat IgG2b (clone LTF-2, BioXCell).

Surgery and KikGR photoconversion

Tumor-bearing animals were anaesthetized with isoflurane, shaved, and washed with ethanol and 0.005 M iodine solution. The tumor was completely exposed by an incision made on the side distal to

the iLN. Photoactivation was performed by exposing the tumor to 415-nm light for 3 min using a custom-built Prizmatix LED source. The incision was then closed using autoclips (Fine Science Tools).

Bone marrow chimeras

WT C57BL6/J mice were lethally irradiated with two doses of 4.5 gray (Gy) from an x-ray source, administered 5 hours apart. Animals were reconstituted by intravenous injection of hematopoietic cells obtained from bone marrow samples of donor mice. Chimeric mice were used in experiments 7 to 12 weeks after irradiation.

Flow cytometry and cell sorting

iLNs were collected and cut into small pieces in microfuge tubes. For digestion, iLNs were incubated for 30 min at 37°C in Hanks' balanced salt solution (HBSS; Gibco) supplemented with $CaCl_2$, $MgCl_2$, and collagenase D (Roche). After digestion, tissue was forced five times through a 21-gauge needle (BD Biosciences) and filtered through a 70-μm strainer into a 15-ml Falcon tube. Tumors were excised, cut into small pieces, and digested with collagenase D and deoxyribonuclease I for 1 hour at 37 °C in HBSS (Gibco). After digestion, tumors were forced 10 times through a 21-gauge needle (BD Biosciences) and filtered through a 70-μm strainer into a 50-ml Falcon tube. Tumors were spun down and resuspended in 3 ml of 10% Percoll/RPMI, which was layered on top of 90% Percoll/RPMI. Cells were spun down for 25 min at 615g at 20°C with brakes off. The gradient interface containing leukocytes was collected and washed with 15 ml of PBS 0.5% bovine serum albumin 1 mM EDTA (PBE) buffer. Single-cell suspensions were washed with PBE and incubated at room temperature for 5 min with anti-CD16/32 (1 μg/ml; 2.4G2, BioXCell). Cells were stained for surface markers on ice in 96-well plates for 15 min in PBE using the reagents listed in table S1. Cells were washed with PBE and stained with Zombie fixable viability dyes (BioLegend) at room temperature for 15 min and then fixed with Cytofix (BD Biosciences). For biotin–LPETG SrtA substrate staining, an antibiotin-phycoerythrin antibody (Miltenyi Biotec) was exclusively used as previously described (28). Samples were acquired on Symphony, Fortessa, or LSR-II flow cytometers or sorted on FACSAria II or FACSAria III cell sorters (BD Biosciences). Data were analyzed using FlowJo v.10.6.2 software.

In vitro lymph node DC–T cell coculture

Mice were injected with the indicated tumors. On day 10, animals were injected with substrate as described above, and biotin+, biotin−, or total migratory DCs from OVA− tumors (150 DCs for OT-II and 500 DCs for OT-I cultures) were sorted into U-bottom 96-well plates; 750 CD4+ OT-II and 2500 CD8+ OT-I CFSE-labeled splenic T cells were sorted in the corresponding wells. All wells contained RPMI supplemented with 1% penicillin/streptomycin, 1% sodium pyruvate, 1% nonessential amino acids, and 1% Hepes. For OT-II cell cultures, RPMI medium was supplemented with 2% T-stim medium with ConA (Avantor). All cells were transferred into fluorescence-activated cell sorting tubes, and the entire sample was recorded to determine cell numbers.

In vitro tumor DC–T cell coculture

Mice were injected with the indicated tumors. On day 10, animals were injected with the substrate intratumorally as described above, and biotin+, biotin−, or total migDCs from OVA− (700 DCs for OT-II and 700 DCs for OT-I cultures) were sorted into U-bottom 96-well plates; 3500 CD4+ OT-II and 3500 CD8+ OT-I CFSE-labeled splenic T cells were sorted in the corresponding wells. All wells contained RPMI supplemented with 1% penicillin/streptomycin, 1% sodium pyruvate, 1% nonessential amino acids, and 1% Hepes.

Library preparation for scRNA-seq and bulk RNA sequencing

Libraries were prepared using the Smart-Seq2 method, as previously described (108). Briefly, RNA from single-sorted cells was extracted using RNAClean XP solid-phase reversible immobilization (SPRI) beads (Beckman Coulter). Extracted RNA was first hybridized using a reverse transcription (RT) primer (/5BiosG/AAGCAGTGGTATCAACG-CAGAGTACTTTTTTTTTTTTTTTTTTTTTTTTTTTTTTTTVN) and then reverse-transcribed into cDNA using a template-switch oligo (TSO) primer (59-AAGCAGTGGTATCAACGCAGAGTACAT-rGrGrG-39) and RT maxima reverse transcriptase (Thermo Fisher Scientific). Amplification of cDNA was performed using an ISPCR primer (59-AAGCAGTGGTATCAACGCAGAGT39) and KAPA HiFi HotStart ReadyMix (Thermo Fisher Scientific). Amplified cDNA was cleaned up three times using RNAClean XP SPRI beads. cDNA was tagmented using the Nextera XT DNA Library Preparation Kit (Illumina). For each sequencing run, up to four plates were barcoded at a time with Nextera XT Index Kit v2 Sets A to D (Illumina). Dual-barcoded libraries were pooled and sequenced using the Illumina NextSeq 550 platform.

Library preparation for scRNA-seq of tumor APCs

scRNA-seq libraries of tumor APCs were prepared by staining cells with oligonucleotide-conjugated antibodies to CD45, MHC-I, and antibiotin for the LIPSTIC signal detection. After sorting, cells were gathered in a microfuge tube containing PBS 0.4% bovine serum albumin, concentrated by centrifugation, and adjusted to a final volume of 35 to 40 μl. Viability counts were performed, and cells were immediately processed for library construction using the Chromium platform (10X Genomics), following the manufacturer's guidelines. The Genomics Core at Rockefeller University carried out the sequencing on an Illumina NovaSeq SP flowcell, aiming for at least 30,000 reads per cell with specific read lengths for each segment of the sequencing process.

Smart-seq2 transcriptomic analysis

Plate-based scRNA-seq libraries were processed by applying the STAR aligner for transcriptome alignment, using the GRCm38.p6 mouse genome assembly and GENCODE M20 mouse annotations. Quantification matrices were produced using RNA-seq by expectation maximization (RSEM). For our single-cell studies, quantification matrices were loaded into the R environment and processed using the Seurat package pipelines (109). Briefly, cells containing more than 10% of their reads mapped to mitochondrial DNA were filtered out. In addition, we removed single-cell contaminants that expressed known markers of B cells, T cells, and macrophages. In total, 552 cells were selected for downstream analysis for our LIPSTIC experiment and 303 cells for our photoactivation experiment. For both experiments, cells were log-normalized, and the top 2000 variable genes were selected for data scaling and principal components analysis (PCA) construction. During data scaling, the library size and the mitochondrial percent variables were regressed out from the postnormalized data. After PCA construction, the JackStraw algorithm available in Seurat was used to select the most significant

principal components. Last, cells were clustered and visualized in *t*-distributed stochastic neighbor embedding (t-SNE) space. For signature analysis, the AddModuleScore function was used to determine the average expression of a gene list compared with a background control. Gene set enrichment analysis was performed in the R environment using the fgsea package (*110*) to determine pathway enrichment. Briefly, fgsea was run using signature sets obtained from MSigDB and used as an input with a preranked list based on the log$_2$ fold change calculated from different pairwise comparisons. Signatures were considered enriched if the adjusted *P* value was at least 0.05. To determine commonly activated genes in LIPSTIC-positive cDC1s and cDC2s, we used a LIPSTIC signature as a pathway and the preranked comparison between cDC1s (positive × negative) and cDC2s (positive × negative). We then compared the two LIPSTIC-positive leading edges for matching and exclusive genes. For external data analysis, data were downloaded from the Gene Expression Omnibus (GEO) database, accession code GSE125680 (*13*). To apply our LIPSTIC signature, we used the AddModuleScore function available with the Seurat package. We used the top 20 genes enriched in biotin-positive DCs compared with biotin-negative DCs or the top 20 genes enriched in cluster 0 compared with the remainder of the cells (*111, 112*).

10X Genomics analysis

The raw fastq files obtained from tumor APC libraries were aligned to the mouse genome (mm39) using the cellranger (v. 7.0.1) pipeline. The quantification matrices were processed in the Seurat (v. 4.0.3) package for R. Briefly, cells containing more than 5% of their transcriptome mapped to mitochondrial reads were removed from downstream analysis. Hashtag counts and biotin antibodies were log-normalized using the NormalizeData function. Cells were classified into their biological conditions on the basis of hashtag quantification using the HTODemux function. Cells containing two or more hashtags were marked as doublets and removed. The enrichR package was used along with the Panglao database (PanglaoDB_Augmented_2021) for identifying non-APCs. Last, the working dataset was generated by normalizing the raw matrix of counts using the SCTransform function. We used the Wilcoxon rank test to generate differentially expressed genes, with only those with Bonferroni-adjusted *P* values of 0.05 or less and log$_2$ fold changes of 0.3 or more considered as significantly expressed. Signature scores were produced by running the AddModuleScore function available in Seurat. The database containing signature lists was obtained from the MSigDB. Pseudotime trajectories were calculated using the Sling-Shot (v. 2.7.0) package for R. Last, to classify cells from our photoactivation experiment produced using smart-seq2 libraries into our 10X Genomics experiment, we used the MapQuery function available in Seurat (5.0.2).

Statistical analysis

All statistical analyses were performed using data from at least three biological replicates, with the exact number of replicates stated in each figure legend. Unless stated otherwise, all statistical analyses were performed using GraphPad Prism v.8 software. Unpaired Student's *t* test was used for most pairwise comparisons, except instances indicated in figure legends where paired Student's *t* test or Wilcoxon signed-rank test was used. For experiments involving more than two groups of animals, one-way analysis of variance (ANOVA) was used with Tukey's test comparing the means of every treatment to the

means of every other treatment. Differences with *P* values < 0.05 were considered statistically significant.

Supplementary Materials

The PDF file includes:
Figs. S1 to S6
Table S1

Other Supplementary Material for this manuscript includes the following:
Data files S1 to S6
MDAR Reproducibility Checklist

REFERENCES AND NOTES

1. D. R. Leach, M. F. Krummel, J. P. Allison, Enhancement of antitumor immunity by CTLA-4 blockade. *Science* **271**, 1734–1736 (1996).

2. P. Sharma, J. P. Allison, Immune checkpoint targeting in cancer therapy: Toward combination strategies with curative potential. *Cell* **161**, 205–214 (2015).

3. V. T. DeVita Jr., S. A. Rosenberg, Two hundred years of cancer research. *N. Engl. J. Med.* **366**, 2207–2214 (2012).

4. A. Chudnovskiy, G. Pasqual, G. D. Victora, Studying interactions between dendritic cells and T cells in vivo. *Curr. Opin. Immunol.* **58**, 24–30 (2019).

5. M. Merad, P. Sathe, J. Helft, J. Miller, A. Mortha, The dendritic cell lineage: Ontogeny and function of dendritic cells and their subsets in the steady state and the inflamed setting. *Annu. Rev. Immunol.* **31**, 563–604 (2013).

6. S. K. Wculek, F. J. Cueto, A. M. Mujal, I. Melero, M. F. Krummel, D. Sancho, Dendritic cells in cancer immunology and immunotherapy. *Nat. Rev. Immunol.* **20**, 7–24 (2020).

7. M. K. Ruhland, E. W. Roberts, E. Cai, A. M. Mujal, K. Marchuk, C. Beppler, D. Nam, N. K. Serwas, M. Binnewies, M. F. Krummel, Visualizing synaptic transfer of tumor antigens among dendritic cells. *Cancer Cell* **37**, 786–799.e5 (2020).

8. T. L. Murphy, G. E. Grajales-Reyes, X. Wu, R. Tussiwand, C. G. Briseño, A. Iwata, N. M. Kretzer, V. Durai, K. M. Murphy, Transcriptional control of dendritic cell development. *Annu. Rev. Immunol.* **34**, 93–119 (2016).

9. K. Hildner, B. T. Edelson, W. E. Purtha, M. Diamond, H. Matsushita, M. Kohyama, B. Calderon, B. U. Schraml, E. R. Unanue, M. S. Diamond, R. D. Schreiber, T. L. Murphy, K. M. Murphy, Batf3 deficiency reveals a critical role for CD8α$^+$ dendritic cells in cytotoxic T cell immunity. *Science* **322**, 1097–1100 (2008).

10. E. W. Roberts, M. L. Broz, M. Binnewies, M. B. Headley, A. E. Nelson, D. M. Wolf, T. Kaisho, D. Bogunovic, N. Bhardwaj, M. F. Krummel, Critical role for CD103$^+$/CD141$^+$ dendritic cells bearing CCR7 for tumor antigen trafficking and priming of T cell immunity in melanoma. *Cancer Cell* **30**, 324–336 (2016).

11. H. Salmon, J. Idoyaga, A. Rahman, M. Leboeuf, R. Remark, S. Jordan, M. Casanova-Acebes, M. Khudoynazarova, J. Agudo, N. Tung, S. Chakarov, C. Rivera, B. Hogstad, M. Bosenberg, D. Hashimoto, S. Gnjatic, N. Bhardwaj, A. K. Palucka, B. D. Brown, J. Brody, F. Ginhoux, M. Merad, Expansion and activation of CD103$^+$ dendritic cell progenitors at the tumor site enhances tumor responses to therapeutic PD-L1 and BRAF inhibition. *Immunity* **44**, 924–938 (2016).

12. S. T. Ferris, V. Durai, R. Wu, D. J. Theisen, J. P. Ward, M. D. Bern, J. T. Davidson IV, P. Bagadia, T. Liu, C. G. Briseño, L. Li, W. E. Gillanders, G. F. Wu, W. M. Yokoyama, T. L. Murphy, R. D. Schreiber, K. M. Murphy, cDC1 prime and are licensed by CD4$^+$ T cells to induce anti-tumour immunity. *Nature* **584**, 624–629 (2020).

13. M. Binnewies, A. M. Mujal, J. L. Pollack, A. J. Combes, E. A. Hardison, K. C. Barry, J. Tsui, M. K. Ruhland, K. Kersten, M. A. Abushawish, M. Spasic, J. P. Giurintano, V. Chan, A. I. Daud, P. Ha, C. J. Ye, E. W. Roberts, M. F. Krummel, Unleashing type-2 dendritic cells to drive protective antitumor CD4$^+$T cell immunity. *Cell* **177**, 556–571.e16 (2019).

14. M. L. Broz, M. Binnewies, B. Boldajipour, A. E. Nelson, J. L. Pollack, D. J. Erle, A. Barczak, M. D. Rosenblum, A. Daud, D. L. Barber, S. Amigorena, L. J. Van't Veer, A. I. Sperling, D. M. Wolf, M. F. Krummel, Dissecting the tumor myeloid compartment reveals rare activating antigen-presenting cells critical for T cell immunity. *Cancer Cell* **26**, 938 (2014).

15. A. R. Sanchez-Paulete, F. J. Cueto, M. Martínez-López, S. Labiano, A. Morales-Kastresana, M. E. Rodríguez-Ruiz, M. Jure-Kunkel, A. Azpilikueta, M. A. Aznar, J. I. Quetglas, D. Sancho, I. Melero, Cancer immunotherapy with immunomodulatory anti-CD137 and anti-PD-1 monoclonal antibodies requires BATF3-dependent dendritic cells. *Cancer Discov.* **6**, 71–79 (2016).

16. S. Spranger, R. Bao, T. F. Gajewski, Melanoma-intrinsic β-catenin signalling prevents anti-tumour immunity. *Nature* **523**, 231–235 (2015).

17. S. Spranger, D. Dai, B. Horton, T. F. Gajewski, Tumor-residing Batf3 dendritic cells are required for effector T cell trafficking and adoptive T cell therapy. *Cancer Cell* **31**, 711–723.e4 (2017).

18. F. Marangoni, A. Zhakyp, M. Corsini, S. N. Geels, E. Carrizosa, M. Thelen, V. Mani, J. N. Prüßmann, R. D. Warner, A. J. Ozga, M. Di Pilato, S. Othy, T. R. Mempel, Expansion of tumor-associated Treg cells upon disruption of a CTLA-4-dependent feedback loop. *Cell* **184**, 3998–4015.e19 (2021).

19. C. S. Garris, S. P. Arlauckas, R. H. Kohler, M. P. Trefny, S. Garren, C. Piot, C. Engblom, C. Pfirschke, M. Siwicki, J. Gungabeesoon, G. J. Freeman, S. E. Warren, S. Ong, E. Browning, C. G. Twitty, R. H. Pierce, M. H. Le, A. P. Algazi, A. I. Daud, S. I. Pai, A. Zippelius, R. Weissleder, M. J. Pittet, Successful anti-PD-1 cancer immunotherapy requires T cell–dendritic cell crosstalk involving the cytokines IFN-γ and IL-12. *Immunity* **49**, 1148–1161.e7 (2018).

20. B. Maier, A. M. Leader, S. T. Chen, N. Tung, C. Chang, J. LeBerichel, A. Chudnovskiy, S. Maskey, L. Walker, J. P. Finnigan, M. E. Kirkling, B. Reizis, S. Ghosh, N. R. D'Amore, N. Bhardwaj, C. V. Rothlin, A. Wolf, R. Flores, T. Marron, A. H. Rahman, E. Kenigsberg, B. D. Brown, M. Merad, A conserved dendritic-cell regulatory program limits antitumour immunity. *Nature* **580**, 257–262 (2020).

21. A. C. Villani, R. Satija, G. Reynolds, S. Sarkizova, K. Shekhar, J. Fletcher, M. Griesbeck, A. Butler, S. Zheng, S. Lazo, L. Jardine, D. Dixon, E. Stephenson, E. Nilsson, I. Grundberg, D. McDonald, A. Filby, W. Li, P. L. De Jager, O. Rozenblatt-Rosen, A. A. Lane, M. Haniffa, A. Regev, N. Hacohen, Single-cell RNA-seq reveals new types of human blood dendritic cells, monocytes, and progenitors. *Science* **356**, eaah4573 (2017).

22. C. A. Dutertre, E. Becht, S. E. Irac, A. Khalilnezhad, V. Narang, S. Khalilnezhad, P. Y. Ng, L. L. van den Hoogen, J. Y. Leong, B. Lee, M. Chevrier, X. M. Zhang, P. J. A. Yong, G. Koh, J. Lum, S. W. Howland, E. Mok, J. Chen, A. Larbi, H. K. K. Tan, T. K. H. Lim, P. Karagianni, A. G. Tzioufas, B. Malleret, J. Brody, S. Albani, J. van Roon, T. Radstake, E. W. Newell, F. Ginhoux, Single-cell analysis of human mononuclear phagocytes reveals subset-defining markers and identifies circulating inflammatory dendritic cells. *Immunity* **51**, 573–589.e8 (2019).

23. F. Ginhoux, M. Guilliams, M. Merad, Expanding dendritic cell nomenclature in the single-cell era. *Nat. Rev. Immunol.* **22**, 67–68 (2022).

24. I. Heras-Murillo, I. Adan-Barrientos, M. Galan, S. K. Wculek, D. Sancho, Dendritic cells as orchestrators of anticancer immunity and immunotherapy. *Nat. Rev. Clin. Oncol.* **21**, 257–277 (2024).

25. M. J. Pittet, M. Di Pilato, C. Garris, T. R. Mempel, Dendritic cells as shepherds of T cell immunity in cancer. *Immunity* **56**, 2218–2230 (2023).

26. A. Del Prete, V. Salvi, A. Soriani, M. Laffranchi, F. Sozio, D. Bosisio, S. Sozzani, Dendritic cell subsets in cancer immunity and tumor antigen sensing. *Cell. Mol. Immunol.* **20**, 432–447 (2023).

27. D. S. Chen, I. Mellman, Oncology meets immunology: The cancer-immunity cycle. *Immunity* **39**, 1–10 (2013).

28. G. Pasqual, A. Chudnovskiy, J. M. J. Tas, M. Agudelo, L. D. Schweitzer, A. Cui, N. Hacohen, G. D. Victora, Monitoring T cell–dendritic cell interactions in vivo by intercellular enzymatic labelling. *Nature* **553**, 496–500 (2018).

29. K. Basso, U. Klein, H. Niu, G. A. Stolovitzky, Y. Tu, A. Califano, G. Cattoretti, R. Dalla-Favera, Tracking CD40 signaling during germinal center development. *Blood* **104**, 4088–4096 (2004).

30. S. Ghosh, M. S. Hayden, New regulators of NF-κB in inflammation. *Nat. Rev. Immunol.* **8**, 837–848 (2008).

31. E. G. Lee, D. L. Boone, S. Chai, S. L. Libby, M. Chien, J. P. Lodolce, A. Ma, Failure to regulate TNF-induced NF-κB and cell death responses in A20-deficient mice. *Science* **289**, 2350–2354 (2000).

32. Q. Peng, X. Qiu, Z. Zhang, S. Zhang, Y. Zhang, Y. Liang, J. Guo, H. Peng, M. Chen, Y. X. Fu, H. Tang, PD-L1 on dendritic cells attenuates T cell activation and regulates response to immune checkpoint blockade. *Nat. Commun.* **11**, 4835 (2020).

33. J. Rossjohn, D. G. Pellicci, O. Patel, L. Gapin, D. I. Godfrey, Recognition of CD1d-restricted antigens by natural killer T cells. *Nat. Rev. Immunol.* **12**, 845–857 (2012).

34. A. W. Zimmerman, B. Joosten, R. Torensma, J. R. Parnes, F. N. van Leeuwen, C. G. Figdor, Long-term engagement of CD6 and ALCAM is essential for T-cell proliferation induced by dendritic cells. *Blood* **107**, 3212–3220 (2006).

35. A. Kumanogoh, T. Shikina, K. Suzuki, S. Uematsu, K. Yukawa, S.-I. Kashiwamura, H. Tsutsui, M. Yamamoto, H. Takamatsu, E. P. Ko-Mitamura, N. Takegahara, S. Marukawa, I. Ishida, H. Morishita, D. V. R. Prasad, M. Tamura, M. Mizui, T. Toyofuku, S. Akira, K. Takeda, M. Okabe, H. Kikutani, Nonredundant roles of Sema4A in the immune system: Defective T cell priming and Th1/Th2 regulation in Sema4A-deficient mice. *Immunity* **22**, 305–316 (2005).

36. M. Groettrup, C. J. Kirk, M. Basler, Proteasomes in immune cells: More than peptide producers? *Nat. Rev. Immunol.* **10**, 73–78 (2010).

37. A. R. Everitt, S. Clare, T. Pertel, S. P. John, R. S. Wash, S. E. Smith, C. R. Chin, E. M. Feeley, J. S. Sims, D. J. Adams, H. M. Wise, L. Kane, D. Goulding, P. Digard, V. Anttila, J. K. Baillie, T. S. Walsh, D. A. Hume, A. Palotie, Y. Xue, V. Colonna, C. Tyler-Smith, J. Dunning, S. B. Gordon, M. O. S. A. I. C. GenISIS Investigators, R. L. Investigators, P. J. Smyth, G. Openshaw, A. L. Dougan, P. K. Brass, IFITM3 restricts the morbidity and mortality associated with influenza. *Nature* **484**, 519–523 (2012).

38. Q. Tran, J. Park, H. Lee, Y. Hong, S. Hong, S. Park, J. Park, S. H. Kim, TMEM39A and human diseases: A brief review. *Toxicol. Res.* **33**, 205–209 (2017).

39. A. Decout, J. D. Katz, S. Venkatraman, A. Ablasser, The cGAS-STING pathway as a therapeutic target in inflammatory diseases. *Nat. Rev. Immunol.* **21**, 548–569 (2021).

40. X. Zhao, A. Sato, C. S. Dela Cruz, M. Linehan, A. Luegering, T. Kucharzik, A. K. Shirakawa, G. Marquez, J. M. Farber, I. Williams, A. Iwasaki, CCL9 is secreted by the follicle-associated epithelium and recruits dome region Peyer's patch CD11b+ dendritic cells. *J. Immunol.* **171**, 2797–2803 (2003).

41. V. Semmling, V. Lukacs-Kornek, C. A. Thaiss, T. Quast, K. Hochheiser, U. Panzer, J. Rossjohn, P. Perlmutter, J. Cao, D. I. Godfrey, P. B. Savage, P. A. Knolle, W. Kolanus, I. Förster, C. Kurts, Alternative cross-priming through CCL17-CCR4-mediated attraction of CTLs toward NKT cell-licensed DCs. *Nat. Immunol.* **11**, 313–320 (2010).

42. A. L. Coelho, M. A. Schaller, C. F. Benjamim, A. Z. Orlofsky, C. M. Hogaboam, S. L. Kunkel, The chemokine CCL6 promotes innate immunity via immune cell activation and recruitment. *J. Immunol.* **179**, 5474–5482 (2007).

43. T. B. Geijtenbeek, S. I. Gringhuis, C-type lectin receptors in the control of T helper cell differentiation. *Nat. Rev. Immunol.* **16**, 433–448 (2016).

44. T. A. Wynn, Type 2 cytokines: Mechanisms and therapeutic strategies. *Nat. Rev. Immunol.* **15**, 271–282 (2015).

45. D. Gatto, K. Wood, I. Caminschi, D. Murphy-Durland, P. Schofield, D. Christ, G. Karupiah, R. Brink, The chemotactic receptor EBI2 regulates the homeostasis, localization and immunological function of splenic dendritic cells. *Nat. Immunol.* **14**, 446–453 (2013).

46. J. Li, E. Lu, T. Yi, J. G. Cyster, EBI2 augments Tfh cell fate by promoting interaction with IL-2-quenching dendritic cells. *Nature* **533**, 110–114 (2016).

47. T. Yi, J. G. Cyster, EBI2-mediated bridging channel positioning supports splenic dendritic cell homeostasis and particulate antigen capture. *eLife* **2**, e00757 (2013).

48. C. C. Brown, H. Gudjonson, Y. Pritykin, D. Deep, V. P. Lavallée, A. Mendoza, R. Fromme, L. Mazutis, C. Ariyan, C. Leslie, D. Pe'er, A. Y. Rudensky, Transcriptional basis of mouse and human dendritic cell heterogeneity. *Cell* **179**, 846–863.e24 (2019).

49. M. Jinushi, Y. Nakazaki, M. Dougan, D. R. Carrasco, M. Mihm, G. Dranoff, MFG-E8-mediated uptake of apoptotic cells by APCs links the pro- and antiinflammatory activities of GM-CSF. *J. Clin. Invest.* **117**, 1902–1913 (2007).

50. M. S. Jeon, A. Atfield, K. Venuprasad, C. Krawczyk, R. Sarao, C. Elly, C. Yang, S. Arya, K. Bachmaier, L. Su, D. Bouchard, R. Jones, M. Gronski, P. Ohashi, T. Wada, D. Bloom, C. G. Fathman, Y.-C. Liu, J. M. Penninger, Essential role of the E3 ubiquitin ligase Cbl-b in T cell anergy induction. *Immunity* **21**, 167–177 (2004).

51. A. Liberzon, C. Birger, H. Thorvaldsdóttir, M. Ghandi, J. P. Mesirov, P. Tamayo, The Molecular Signatures Database (MSigDB) hallmark gene set collection. *Cell Syst.* **1**, 417–425 (2015).

52. A. Subramanian, P. Tamayo, V. K. Mootha, S. Mukherjee, B. L. Ebert, M. A. Gillette, A. Paulovich, S. L. Pomeroy, T. R. Golub, E. S. Lander, J. P. Mesirov, Gene set enrichment analysis: A knowledge-based approach for interpreting genome-wide expression profiles. *Proc. Natl. Acad. Sci. U.S.A.* **102**, 15545–15550 (2005).

53. R. Zilionis, C. Engblom, C. Pfirschke, V. Savova, D. Zemmour, H. D. Saatcioglu, I. Krishnan, G. Maroni, C. V. Meyerovitz, C. M. Kerwin, S. Choi, W. G. Richards, A. De Rienzo, D. G. Tenen, R. Bueno, E. Levantini, M. J. Pittet, A. M. Klein, Single-cell transcriptomics of human and mouse lung cancers reveals conserved myeloid populations across individuals and species. *Immunity* **50**, 1317–1334.e10 (2019).

54. T. H. Corbett, D. P. Griswold Jr., B. J. Roberts, J. C. Peckham, F. M. Schabel Jr., Tumor induction relationships in development of transplantable cancers of the colon in mice for chemotherapy assays, with a note on carcinogen structure. *Cancer Res* **35**, 2434–2439 (1975).

55. H. Yoshida, C. A. Hunter, The immunobiology of interleukin-27. *Annu. Rev. Immunol.* **33**, 417–443 (2015).

56. M. Fabbi, G. Carbotti, S. Ferrini, Dual roles of IL-27 in cancer biology and immunotherapy. *Mediators Inflamm.* **2017**, 3958069 (2017).

57. N. Chihara, A. Madi, T. Kondo, H. Zhang, N. Acharya, M. Singer, J. Nyman, N. D. Marjanovic, M. S. Kowalczyk, C. Wang, S. Kurtulus, T. Law, Y. Etminan, J. Nevin, C. D. Buckley, P. R. Burkett, J. D. Buenrostro, O. Rozenblatt-Rosen, A. C. Anderson, A. Regev, V. K. Kuchroo, Induction and transcriptional regulation of the co-inhibitory gene module in T cells. *Nature* **558**, 454–459 (2018).

58. J. Zhu, J. Q. Liu, M. Shi, X. Cheng, M. Ding, J. C. Zhang, J. P. Davis, S. Varikuti, A. R. Satoskar, L. Lu, X. Pan, P. Zheng, Y. Liu, X. F. Bai, IL-27 gene therapy induces depletion of Tregs and enhances the efficacy of cancer immunotherapy. *JCI Insight* **3**, e98745 (2018).

59. J. R. Groom, J. Richmond, T. T. Murooka, E. W. Sorensen, J. H. Sung, K. Bankert, U. H. von Andrian, J. J. Moon, T. R. Mempel, A. D. Luster, CXCR3 chemokine receptor-ligand interactions in the lymph node optimize CD4+ T helper 1 cell differentiation. *Immunity* **37**, 1091–1103 (2012).

60. M. E. Mikucki, D. T. Fisher, J. Matsuzaki, J. J. Skitzki, N. B. Gaulin, J. B. Muhitch, A. W. Ku, J. G. Frelinger, K. Odunsi, T. F. Gajewski, A. D. Luster, S. S. Evans, Non-redundant requirement for CXCR3 signalling during tumoricidal T-cell trafficking across tumour vascular checkpoints. *Nat. Commun.* **6**, 7458 (2015).

61. A. Magen, P. Hamon, N. Fiaschi, B. Y. Soong, M. D. Park, R. Mattiuz, E. Humblin, L. Troncoso, D. D'souza, T. Dawson, J. Kim, S. Hamel, M. Buckup, C. Chang, A. Tabachnikova, H. Schwartz, N. Malissen, Y. Lavin, A. Soares-Schanoski, B. Giotti, S. Hegde, G. Ioannou, E. Gonzalez-Kozlova, C. Hennequin, J. Le Berichel, Z. Zhao, S. C. Ward, I. Fiel, B. Kou, M. Dobosz, L. Li, C. Adler, M. Ni, Y. Wei, W. Wang, G. S. Atwal, K. Kundu, K. J. Cygan, A. M. Tsankov, A. Rahman, C. Price, N. Fernandez, J. He, N. T. Gupta, S. Kim-Schulze, S. Gnjatic, E. Kenigsberg, R. P. Deering, M. Schwartz, T. U. Marron, G. Thurston, A. O. Kamphorst, M. Merad, Intratumoral dendritic cell-CD4+ T helper cell niches enable CD8+ T cell differentiation following PD-1 blockade in hepatocellular carcinoma. *Nat. Med.* **29**, 1389–1399 (2023).

62. S. Nakandakari-Higa, S. Walker, M. C. C. Canesso, V. van der Heide, A. Chudnovskiy, D. Y. Kim, J. T. Jacobsen, R. Parsa, J. Bilanovic, S. M. Parigi, K. Fiedorczuk, E. Fuchs, A. M. Bilate, G. Pasqual, D. Mucida, A. O. Kamphorst, Y. Pritykin, G. D. Victora, Universal recording of immune cell interactions in vivo. *Nature* **627**, 399–406 (2024).

63. A. Rizzitelli, S. Meuter, J. Vega Ramos, C. H. Bird, J. D. Mintern, M. S. J. Mangan, J. Villadangos, P. I. Bird, Serpinb9 (Spi6)-deficient mice are impaired in dendritic cell-mediated antigen cross-presentation. *Immunol. Cell. Biol.* **90**, 841–851 (2012).

64. N. Pishesha, T. J. Harmand, H. L. Ploegh, A guide to antigen processing and presentation. *Nat. Rev. Immunol.* **22**, 751–764 (2022).

65. J. R. Arron, Y. Pewzner-Jung, M. C. Walsh, T. Kobayashi, Y. Choi, Regulation of the subcellular localization of tumor necrosis factor receptor-associated factor (TRAF)2 by TRAF1 reveals mechanisms of TRAF2 signaling. *J. Exp. Med.* **196**, 923–934 (2002).

66. G. Donninelli, I. Sanseverino, C. Purificato, S. Gessani, M. C. Gauzzi, Dual requirement for STAT signaling in dendritic cell immunobiology. *Immunobiology* **223**, 342–347 (2018).

67. L. Chen, D. B. Flies, Molecular mechanisms of T cell co-stimulation and co-inhibition. *Nat. Rev. Immunol.* **13**, 227–242 (2013).

68. M. Di Pilato, R. Kfuri-Rubens, J. N. Pruessmann, A. J. Ozga, M. Messemaker, B. L. Cadilha, R. Sivakumar, C. Cianciaruso, R. D. Warner, F. Marangoni, E. Carrizosa, S. Lesch, J. Billingsley, D. Perez-Ramos, F. Zavala, E. Rheinbay, A. D. Luster, M. Y. Gerner, S. Kobold, M. J. Pittet, T. R. Mempel, CXCR6 positions cytotoxic T cells to receive critical survival signals in the tumor microenvironment. *Cell* **184**, 4512–4530.e22 (2021).

69. J. Wei, S. Xia, H. Sun, S. Zhang, J. Wang, H. Zhao, X. Wu, X. Chen, J. Hao, X. Zhou, Z. Zhu, X. Gao, J. X. Gao, P. Wang, Z. Wu, L. Zhao, Z. Yin, Critical role of dendritic cell-derived IL-27 in antitumor immunity through regulating the recruitment and activation of NK and NKT cells. *J. Immunol.* **191**, 500–508 (2013).

70. M. Kitano, C. Yamazaki, A. Takumi, T. Ikeno, H. Hemmi, N. Takahashi, K. Shimizu, S. E. Fraser, K. Hoshino, T. Kaisho, T. Okada, Imaging of the cross-presenting dendritic cell subsets in the skin-draining lymph node. *Proc. Natl. Acad. Sci. U.S.A.* **113**, 1044–1049 (2016).

71. S. Nowotschin, A. K. Hadjantonakis, Use of KikGR a photoconvertible green-to-red fluorescent protein for cell labeling and lineage analysis in ES cells and mouse embryos. *BMC Dev. Biol.* **9**, 49 (2009).

72. H. Tsutsui, S. Karasawa, H. Shimizu, N. Nukina, A. Miyawaki, Semi-rational engineering of a coral fluorescent protein into an efficient highlighter. *EMBO Rep.* **6**, 233–238 (2005).

73. C. Y. C. Lee, B. C. Kennedy, N. Richoz, I. Dean, Z. K. Tuong, Z. Li, C. Willis, T. Hasegawa, S. K. Whiteside, D. A. Posner, G. Carlesso, S. A. Hammond, S. J. Dovedi, R. Roychoudhuri, D. R. Withers, M. R. Clatworthy, Tumour-retained activated CCR7+ dendritic cells are heterogeneous and regulate local anti-tumour cytolytic activity. *Nat. Commun.* **15**, 682 (2024).

74. I. Mellman, D. S. Chen, T. Powles, S. J. Turley, The cancer-immunity cycle: Indication, genotype, and immunotype. *Immunity* **56**, 2188–2205 (2023).

75. D. M. Pardoll, The blockade of immune checkpoints in cancer immunotherapy. *Nat. Rev. Cancer.* **12**, 252–264 (2012).

76. B. Chen, L. Zhu, S. Yang, W. Su, Unraveling the heterogeneity and ontogeny of dendritic cells using single-cell RNA sequencing. *Front. Immunol.* **12**, 711329 (2021).

77. D. Esterházy, J. Loschko, M. London, V. Jove, T. Y. Oliveira, D. Mucida, Classical dendritic cells are required for dietary antigen-mediated induction of peripheral T$_{reg}$ cells and tolerance. *Nat. Immunol.* **17**, 545–555 (2016).

78. A. Giladi, M. Cohen, C. Medaglia, Y. Baran, B. Li, M. Zada, P. Bost, R. Blecher-Gonen, T. M. Salame, J. U. Mayer, E. David, F. Ronchese, A. Tanay, I. Amit, Dissecting cellular crosstalk by sequencing physically interacting cells. *Nat. Biotechnol.* **38**, 629–637 (2020).

79. J. D. Altman, P. A. Moss, P. J. Goulder, D. H. Barouch, M. G. McHeyzer-Williams, J. I. Bell, A. J. McMichael, M. M. Davis, Phenotypic analysis of antigen-specific T lymphocytes. *Science* **274**, 94–96 (1996).

80. A. T. Krishnamurty, C. D. Thouvenel, S. Portugal, G. J. Keitany, K. S. Kim, A. Holder, P. D. Crompton, D. J. Rawlings, M. Pepper, Somatically hypermutated *Plasmodium*-specific IgM+ memory B cells are rapid, plastic, early responders upon malaria rechallenge. *Immunity* **45**, 402–414 (2016).

81. M. Cohen, A. Giladi, O. Barboy, P. Hamon, B. Li, M. Zada, A. Gurevich-Shapiro, C. G. Beccaria, E. David, B. B. Maier, M. Buckup, I. Kamer, A. Deczkowska, J. Le Berichel, J. Bar, M. Iannacone, A. Tanay, M. Merad, I. Amit, The interaction of CD4+ helper T cells with dendritic cells shapes the tumor microenvironment and immune checkpoint blockade response. *Nat. Cancer* **3**, 303–317 (2022).

82. R. Lesley, L. M. Kelly, Y. Xu, J. G. Cyster, Naive CD4 T cells constitutively express CD40L and augment autoreactive B cell survival. *Proc. Natl. Acad. Sci. U.S.A.* **103**, 10717–10722 (2006).

83. I. S. Grewal, R. A. Flavell, The role of CD40 ligand in costimulation and T-cell activation. *Immunol. Rev.* **153**, 85–106 (1996).

84. A. Döhler, T. Schneider, I. Eckert, E. Ribechini, N. Andreas, M. Riemann, B. Reizis, F. Weih, M. B. Lutz, RelB+steady-state migratory dendritic cells control the peripheral pool of the natural Foxp3+ regulatory T cells. *Front. Immunol.* **8**, 726 (2017).

85. J. Borst, T. Ahrends, N. Babala, C. J. M. Melief, W. Kastenmuller, CD4+ T cell help in cancer immunology and immunotherapy. *Nat. Rev. Immunol.* **18**, 635–647 (2018).

86. S. R. Bennett, F. R. Carbone, F. Karamalis, R. A. Flavell, J. F. Miller, W. R. Heath, Help for cytotoxic-T-cell responses is mediated by CD40 signalling. *Nature* **393**, 478–480 (1998).

87. S. P. Schoenberger, R. E. Toes, E. I. van der Voort, R. Offringa, C. J. Melief, T-cell help for cytotoxic T lymphocytes is mediated by CD40-CD40L interactions. *Nature* **393**, 480–483 (1998).

88. J. P. Ridge, F. Di Rosa, P. Matzinger, A conditioned dendritic cell can be a temporal bridge between a CD4+ T-helper and a T-killer cell. *Nature* **393**, 474–478 (1998).

89. J. Bancherau, R. M. Steinman, Dendritic cells and the control of immunity. *Nature* **392**, 245–252 (1998).

90. I. Mellman, R. M. Steinman, Dendritic cells: Specialized and regulated antigen processing machines. *Cell* **106**, 255–258 (2001).

91. M. M. S. Oliveira, L. S. Westerberg, Cytoskeletal regulation of dendritic cells: An intricate balance between migration and presentation for tumor therapy. *J. Leukoc. Biol.* **108**, 1051–1065 (2020).

92. F. Castellino, A. Y. Huang, G. Altan-Bonnet, S. Stoll, C. Scheinecker, R. N. Germain, Chemokines enhance immunity by guiding naive CD8+ T cells to sites of CD4+ T cell-dendritic cell interaction. *Nature* **440**, 890–895 (2006).

93. G. Murugaiyan, B. Saha, IL-27 in tumor immunity and immunotherapy. *Trends Mol. Med.* **19**, 108–116 (2013).

94. A. Hu, M. Ding, J. Zhu, J. Q. Liu, X. Pan, K. Ghoshal, X. F. Bai, Intra-tumoral delivery of IL-27 using adeno-associated virus stimulates anti-tumor immunity and enhances the efficacy of immunotherapy. *Front. Cell Dev. Biol.* **8**, 210 (2020).

95. A. M. Kilgore, S. Welsh, E. E. Cheney, A. Chitrakar, T. J. Blain, B. J. Kedl, C. A. Hunter, N. D. Pennock, R. M. Kedl, IL-27p28 production by XCR1+ dendritic cells and monocytes effectively predicts adjuvant-elicited CD8+ T cell responses. *Immunohorizons* **2**, 1–11 (2018).

96. N. D. Pennock, L. Gapin, R. M. Kedl, IL-27 is required for shaping the magnitude, affinity distribution, and memory of T cells responding to subunit immunization. *Proc. Natl. Acad. Sci. U.S.A.* **111**, 16472–16477 (2014).

97. G. M. Gerhard, R. Bill, M. Messemaker, A. M. Klein, M. J. Pittet, Tumor-infiltrating dendritic cell states are conserved across solid human cancers. *J. Exp. Med.* **218**, e20200264 (2021).

98. P. S. Liu, Y. T. Chen, X. Li, P. C. Hsueh, S. F. Tzeng, H. Chen, P. Z. Shi, X. Xie, S. Parik, M. Planque, S. M. Fendt, P. C. Ho, CD40 signal rewires fatty acid and glutamine metabolism for stimulating macrophage anti-tumorigenic functions. *Nat. Immunol.* **24**, 452–462 (2023).

99. P. Sharma, J. P. Allison, Dissecting the mechanisms of immune checkpoint therapy. *Nat. Rev. Immunol.* **20**, 75–76 (2020).

100. L. Madsen, N. Labrecque, J. Engberg, A. Dierich, A. Svejgaard, C. Benoist, D. Mathis, L. Fugger, Mice lacking all conventional MHC class II genes. *Proc. Natl. Acad. Sci. U.S.A.* **96**, 10338–10343 (1999).

101. P. P. Lee, D. R. Fitzpatrick, C. Beard, H. K. Jessup, S. Lehar, K. W. Makar, M. Pérez-Melgosa, M. T. Sweetser, M. S. Schlissel, S. Nguyen, S. R. Cherry, J. H. Tsai, S. M. Tucker, W. M. Weaver, A. Kelso, R. Jaenisch, C. B. Wilson, A critical role for Dnmt1 and DNA methylation in T cell development, function, and survival. *Immunity* **15**, 763–774 (2001).

102. K. A. Hogquist, S. C. Jameson, W. R. Heath, J. L. Howard, M. J. Bevan, F. R. Carbone, T cell receptor antagonist peptides induce positive selection. *Cell* **76**, 17–27 (1994).

103. M. J. Barnden, J. Allison, W. R. Heath, F. R. Carbone, Defective TCR expression in transgenic mice constructed using cDNA-based α- and β-chain genes under the control of heterologous regulatory elements. *Immunol. Cell Biol.* **76**, 34–40 (1998).

104. M. L. Caton, M. R. Smith-Raska, B. Reizis, Notch-RBP-J signaling controls the homeostasis of CD8- dendritic cells in the spleen. *J. Exp. Med.* **204**, 1653–1664 (2007).

105. R. M. Quadros, H. Miura, D. W. Harms, H. Akatsuka, T. Sato, T. Aida, R. Redder, G. P. Richardson, Y. Inagaki, D. Sakai, S. M. Buckley, P. Seshacharyulu, S. K. Batra, M. A. Behlke, S. A. Zeiner, A. M. Jacobi, Y. Izu, W. B. Thoreson, L. D. Urness, S. L. Mansour, M. Ohtsuka, C. B. Gurumurthy, Easi-CRISPR: A robust method for one-step generation of mice carrying conditional and insertion alleles using long ssDNA donors and CRISPR ribonucleoproteins. *Genome Biol.* **18**, 92 (2017).

106. B. Engels, H. Cam, T. Schüler, S. Indraccolo, M. Gladow, C. Baum, T. Blankenstein, W. Uckert, Retroviral vectors for high-level transgene expression in T lymphocytes. *Hum. Gene Ther.* **14**, 1155–1168 (2003).

107. A. L. Szymczak, D. A. Vignali, Development of 2A peptide-based strategies in the design of multicistronic vectors. *Expert Opin. Biol. Ther.* **5**, 627–638 (2005).

108. J. J. Trombetta, D. Gennert, D. Lu, R. Satija, A. K. Shalek, A. Regev, Preparation of single-cell RNA-seq libraries for next generation sequencing. *Curr. Protoc. Mol. Biol.* **107**, 4.22.1–4.22.17 (2014).

109. Y. Hao, S. Hao, E. Andersen-Nissen, W. M. Mauck III, S. Zheng, A. Butler, M. J. Lee, A. J. Wilk, C. Darby, M. Zager, P. Hoffman, M. Stoeckius, E. Papalexi, E. P. Mimitou, J. Jain, A. Srivastava, T. Stuart, L. M. Fleming, B. Yeung, A. J. Rogers, Integrated analysis of multimodal single-cell data. *Cell* **184**, 3573–3587.e29 (2021).

110. G. Korotkevich, V. Sukhov, N. Budin, B. Shpak, M. N. Artyomov, A. Sergushichev, Fast gene set enrichment analysis. bioRxiv 060012 [Preprint] (2021). https://doi.org/10.1101/060012.

111. M. Stephens, False discovery rates: A new deal. *Biostatistics* **18**, 275–294 (2017).

112. M. I. Love, W. Huber, S. Anders, Moderated estimation of fold change and dispersion for RNA-seq data with DESeq2. *Genome Biol.* **15**, 550 (2014).